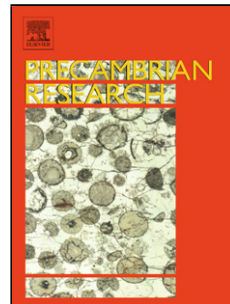


Accepted Manuscript

Title: Neoproterozoic subduction along the Ailaoshan zone, South China: Geochronological and geochemical evidence from amphibolite



Author: Yongfeng Cai Yuejun Wang Peter A. Cawood
Weiming Fan Huichuan Liu Xiaowan Xing Yuzhi Zhang

PII: S0301-9268(14)00028-X

DOI: <http://dx.doi.org/doi:10.1016/j.precamres.2014.01.009>

Reference: PRECAM 3918

To appear in: *Precambrian Research*

Received date: 28-10-2013

Revised date: 22-1-2014

Accepted date: 24-1-2014

Please cite this article as: Wang, Y.C., Y., Cawood, P.A., Fan, W., Liu, H., Xing, X., Zhang, Y., Neoproterozoic subduction along the Ailaoshan zone, South China: geochronological and geochemical evidence from amphibolite, *Precambrian Research* (2014), <http://dx.doi.org/10.1016/j.precamres.2014.01.009>

This is a PDF file of an unedited manuscript that has been accepted for publication. As a service to our customers we are providing this early version of the manuscript. The manuscript will undergo copyediting, typesetting, and review of the resulting proof before it is published in its final form. Please note that during the production process errors may be discovered which could affect the content, and all legal disclaimers that apply to the journal pertain.

1

2

3

4 Neoproterozoic subduction along the Ailaoshan zone, South China: 5 geochronological and geochemical evidence from amphibolite

Yongfeng Cai^{1, 2, 3} Yuejun Wang^{2, 4,*} Peter A. Cawood^{5, 6}
 Weiming Fan¹ Huichuan Liu^{1, 3} Xiaowan Xing^{1, 3} Yuzhi Zhang¹

1 State Key Laboratory of Isotope Geochemistry, Guangzhou Institute of Geochemistry, Chinese
2 Academy of Sciences, Guangzhou 510640, China

¹⁴ 2 Department of Earth Sciences, Sun Yat-Sen University, Guangzhou, China

¹⁵ 3 University of Chinese Academy of Sciences, Beijing 100049, China

4 Guangdong Provincial Key Laboratory of Mineral Resources and Geological Processes,
Guangzhou, 510275, China

5 Department of Earth Sciences, University of St Andrews, North Street, St Andrews KY16 9AL,
UK

6 School of Earth and Environment, University of Western Australia, 35 Stirling Highway, Crawley,
WA 6009, Australia

25 * Corresponding author

26 Department of Earth Sciences

27 Sun Yat-Sen University

28 No. 135, Xingang Xi Road, Guangzhou, 510275

29 People's Republic of China

30 Tel: 86-20-84111209

31 Email: wangyuejun@m

32

33

34 **Abstract:** Lenses of amphibolites occur along the Ailaoshan suture zone at the
35 southwestern margin of the Yangtze Block, South China. Petrological, geochemical and
36 zircon U–Pb geochronological data indicate that they are divisible into two coeval groups.
37 Group 1, represented by the Jinping amphibolite, has mg-number of 71~76 and (La/Yb)cn
38 ratios of 7.2~7.7, and displays a geochemical affinity to island arc volcanic rocks. Group 2
39 amphibolites occur at Yuanyang and are characterized by high Nb contents (14.3~18.4 ppm),
40 resembling Nb-enriched basalts. The $\varepsilon_{\text{Nd}}(t)$ values for Group 1 range from -3.45 to -2.04 and
41 for Group 2 from +4.08 to +4.39. A representative sample for Group 1 yields a U-Pb zircon
42 age of 803 ± 7 Ma, whereas two samples for Group 2 give U-Pb zircon ages of 813 ± 11 Ma
43 and 814 ± 12 Ma. Petrogenetic analysis suggests that Group 1 originated from an
44 orthopyroxene-rich source and Group 2 from a mantle wedge modified by slab-derived melt.
45 In combination with other geological observations, these amphibolites are inferred to
46 constitute part of an early Neoproterozoic (~815~800 Ma) arc-back-arc basin system. The
47 Neoproterozoic amphibolites and related rocks along the Ailaoshan zone may be the
48 southward extension of the Neoproterozoic supra-subduction zone that developed along the
49 western margin of the Yangtze Block.

50 **Keywords:** Ailaoshan zone; amphibolite; zircon U-Pb dating; petrogenesis; Neoproterozoic
51 subduction

52

53 **1. Introduction**

54 The position of South China Craton (SCC) has played a key role in paleogeographic
55 models for assembly of Precambrian supercontinents and contrasting intracratonic and

56 peripheral locations have been proposed (e.g., Cawood et al., 2013; Li et al., 1995, 2008a;
57 Yan et al., 2004; Zhao and Cawood, 1999, Zhao and Guo, 2012; Zhou et al., 2002a). Key to
58 resolving this controversy is to understand the tectonic setting of Neoproterozoic igneous
59 rocks within the SCC, and whether they formed in supra-subduction zone and/or
60 within-plate environments. These Neoproterozoic igneous rocks are mainly distributed
61 along the northern, western and eastern margins of the Yangtze Block and their petrogenesis
62 and tectonic environment has been a focus of intense study and debate (e.g., Chen et al.,
63 2013; Dong et al., 2011, 2012; Li et al., 2002; 2003a; Zhang et al., 2013b; Zhao and
64 Cawood, 2012; Zhao et al., 2011; Zhou et al., 2002a, 2006b). In this study, we document the
65 petrological characteristics, geochemical affinities and tectonic setting of the
66 newly-identified Neoproterozoic amphibolites along the Ailaoshan zone adjacent to the
67 southwestern margin of the Yangtze Block. These data indicate a supra-subduction zone
68 setting and constrain the Neoproterozoic location of South China to a position along the
69 northern margin of the Rodinia supercontinent.

70

71 **2. Geological Setting**

72 The Ailaoshan suture zone forms part of a major tectonic zone that marks the southern
73 boundary of the SCC (Fig. 1). It can be traced for at least 300 km and is up to 30 km wide in
74 Yunnan Province, SW China. The zone was reactivated in the late Paleozoic to early
75 Mesozoic during closure of the Tethys Ocean and resultant accretion of the Indochina Block
76 to the southeast of the suture zone (e.g., Charvet et al., 1996; Zhong, 1998). Subsequent
77 strike-slip deformation associated with the India-Asia collision during the Cenozoic period

78 reactivated the Ailaoshan suture zone and further disrupted it into a series of faults, e.g., Red
79 River, Ailaoshan, Jiujia-Anding, Lixiangjiang and Tengtiaohe faults (Fig. 2, e.g., Tapponier
80 et al., 1990).

81 The Cenozoic Ailaoshan Fault divides the suture zone into two lithotectonic
82 successions (Fig. 2). To the northeast of the fault is a high-grade metamorphic succession of
83 sillimanite-biotite gneiss, two-mica schist, amphibolite, biotite-amphibole-plagioclase
84 gneiss, graphite-quartz marble, biotite gneiss, graphite schist, which together are defined as
85 the Precambrian Ailaoshan Group/Complex (e.g., Lu, 1989; Yunnan BGMR, 1983; Zhong,
86 1998). To the southwest of the fault occurs a greenschist facies association of Paleozoic and
87 earliest Mesozoic sedimentary and igneous rocks, including Permian ophiolitic fragments
88 (Fan et al., 2010; Yunnan BGMR, 1983; Zhong, 1998). The Ailaoshan suture zone abuts the
89 Yangtze Block (Figs. 1-2) that comprises Archean to Paleoproterozoic crystalline basement
90 and Neoproterozoic to lower Paleozoic and upper Paleozoic marine packages (e.g., Cawood
91 et al., 2013; Qiu and Gao, 2000; Wang et al., 2013a; Zhao and Cawood, 2012).

92 Within the Ailaoshan Group/Complex are small outcrops of mafic and ultramafic rocks
93 that occur as lens, pods and isolated fragments. They consist mainly of hornblende
94 pyroxenite, amphibolite and metagabbro, and peridotite and pyroxenite, and were previously
95 considered to be Paleoproterozoic to Mesoproterozoic in age (e.g., Lu, 1989; Yunnan
96 BGMR, 1983). Amphibolite is the dominant rock type and is the focus of this study. It is
97 best developed in the Jinping and Yuanyang areas (Fig. 2b, c). The amphibolites at Jinping,
98 named herein Group 1, show blastoporphyritic texture and banded structure and are
99 composed of pleochroic hornblende (~40-50 %), plagioclase (~30-45 %), quartz (~5 %),

100 biotite (~3 %) and small amounts of clinzoisite, chlorite, epidote, zircon, apatite and
101 magnetite (Fig. 3a). The amphibolite at Yuanyang, named herein Group 2, display
102 porphyroblastic texture and massive structure with the primary igneous textures often
103 destroyed by later deformation and metamorphism. They consist of pleochroic hornblende
104 (~50-60 %), plagioclase (~20-30 %), pyroxene (~3 %), quartz (~3 %), biotite (~2 %) and
105 small amounts of chlorite, epidote, magnetite, zircon and apatite (Fig. 3b).

106

107 **3. Analytical methods**

108 Zircon grains were extracted from three representative samples of amphibolites
109 (10HH-67A, 10HH-31A and 10HH-67B) by conventional heavy liquid and magnetic
110 techniques. These grains, together with zircon standard 91500, were mounted in epoxy.
111 Transmitted and reflected light micrographs, along with cathodoluminescence (CL) images
112 were taken to display the internal structure of all analyzed grains.

113 U-Th-Pb measurements for 10HH-67A were undertaken using the Cameca IMS-1280
114 SIMS at the Institute of Geology and Geophysics, Chinese Academy of Sciences (CAS).
115 U-Th-Pb absolute abundances and ratios were determined relative to the standard zircon
116 91500 (Wiedenbeck et al., 1995). Detailed description of operating conditions and data
117 processing procedures is given in Li et al. (2009a). The long-term uncertainty for $^{206}\text{Pb}/^{238}\text{U}$
118 measurements of the zircon standard of 1.5% (1 relative standard deviation, RSD) was
119 propagated to the unknown zircons, although in our analytical sessions the measured
120 $^{206}\text{Pb}/^{238}\text{U}$ error was usually about 1% (1 RSD) or less. Non-radiogenic ^{204}Pb was used for
121 the common Pb correction. Corrections are sufficiently small to be insensitive to the choice

122 of common Pb composition, and an average of present-day crustal composition (Stacey and
123 Kramers, 1975) is used for the common Pb assuming that the common Pb is mainly due to
124 surface contamination introduced during sample preparation. Uncertainties on individual
125 analyses in data tables are reported at 1 sigma level and mean ages for pooled Pb/Pb (and
126 U/Pb) analyses are quoted at the 95% confidence interval.

127 The zircon U-Pb isotopic results for samples 10HH-31A and 10HH-67B were analyzed
128 with a VG PlasmaQuad Excell inductively coupled plasma-mass spectrometer (ICP-MS)
129 equipped with a New Wave Research LUV213 laser ablation system at the University of
130 Hong Kong. Analytical settings were a beam diameter of ca. 40 μm , a 10 Hz repetition rate,
131 and energy of 0.6 mJ to 1.3 mJ per pulse. The equipment was tuned with total U signals
132 ranging from 3×10^4 to 100×10^4 counts, depending on U contents. Typical ablation time
133 was 30 s to 60 s, leading to pits of 20 μm to 40 μm deep. Helium carrier gas transported the
134 ablated sample materials from the laser-ablation cell via a mixing chamber to the ICPMS
135 after mixing with Ar gas. The detailed analytical procedure of Xia et al. (2004) is followed.
136 Data reduction for all samples was carried out using the Isoplot/Ex v. 3 program (Ludwig,
137 2001). The U-Pb dating results and sampling locations for 10HH-31A, 10HH-67A and
138 10HH-67B are listed in Table 1 and shown in Figures 2b-c.

139 For whole-rock elemental and isotopic analysis, the representative samples were
140 pulverised to 200-mesh. Major element oxides were analyzed at the Guangzhou Institute of
141 Geochemistry (GIG), CAS, by a wavelength X-ray fluorescence spectrometry using a
142 Rigaku ZSX100e spectrometer with the relative standard derivations of <5 %. Trace element
143 contents were measured using Perkin-Elmer Sciex ELAN 6000 ICP-MS at the GIG, CAS.

144 Detailed sample preparation and analytical procedure of Qi et al. (2000) is followed. Sample
145 powders for Sr and Nd isotopic analyses were spiked with mixed isotope tracers, dissolved
146 in Teflon capsules with HF+HNO₃ acids, and separated by conventional cation-exchange
147 technique and run on single W and Ta-Re double filaments. Sr-Nd isotope ratios were
148 measured on a MicroMass Isoprobe MC-ICP-MS at the GIG, CAS. Sample preparation and
149 chemical separation followed Liang et al. (2003). The total procedure blanks for Sr were
150 200-500 pg and < 50 pg for Nd. ⁸⁶Sr/⁸⁸Sr = 0.1194 and ¹⁴⁶Nd/¹⁴⁴Nd = 0.7219 were used for
151 correcting the mass fractionation for Sr and Nd isotopic ratios, respectively. The measured
152 ⁸⁷Sr/⁸⁶Sr ratio of the (NIST) SRM 987 standard and ¹⁴³Nd/¹⁴⁴Nd ratio of the La Jolla
153 standard is 0.710265 ± 12 (2σ) and 0.511862 ± 10 (2σ), respectively. Within-run errors of
154 precision are estimated to be better than 0.000015 for ⁸⁶Sr/⁸⁸Sr and ¹⁴⁶Nd/¹⁴⁴Nd in the 95%
155 confidence level during the analytical process. The analytical results of major oxides,
156 elements and Sr-Nd isotopes are shown in Tables 2 and 3.

157

158 **4. Results**

159 **4.1. Zircon U-Pb geochronology**

160 Zircons from samples 10HH-31A, 10HH-67A and 10HH-67B are generally transparent
161 to translucent, light-brown to colorless grains or grain fragments with subhedral
162 morphology. They are ~80-120 μm in length with length to width ratios of 1.5:1 to 3:1. CL
163 images exhibit weak oscillatory zoning with variable luminescence, indicative of an igneous
164 origin (Fig. 4a-c).

165 **10HH-31A:** Zircon grains have U contents ranging from 117 ppm to 1138 ppm and Th

166 from 136 to 571 ppm. Their Th/U ratios are in range of 0.49-1.78 (Table 1). Twenty-four
167 analyses on 23 grains form a coherent cluster and give a $^{206}\text{Pb}/^{238}\text{U}$ weighted mean age of
168 803 ± 7 Ma with MSWD = 0.99 (Fig. 4a). In combination with the oscillatory zoning of the
169 grains, this age can be interpreted as the formation age of the sample.

170 **10HH-67A:** The U and Th concentrations for the sixteen analyzed grains range from
171 139 to 1288 ppm and 48 to 3400 ppm, respectively, with Th/U ratios of 0.28-1.03 (Table 1).
172 Most of the analyses are variably discordant, interpreted to be the result of late Pb loss. Four
173 spots yield a coherent group with the $^{206}\text{Pb}/^{238}\text{U}$ weighted mean age of 813 ± 11 Ma with
174 MSWD = 1.05 (Fig. 4b), representing the crystallization age of the sample.

175 **10HH-67B:** Twenty-six analyses on 26 grains exhibit a relatively wide range of U and
176 Th concentrations with U = 112-1608 ppm and Th = 55-542 ppm. Th/U ratios range from
177 0.10 to 1.20 (Table 1). The majority of the 26 analyses form a normally discordant array
178 with the apparent $^{207}\text{Pb}/^{206}\text{Pb} > ^{207}\text{Pb}/^{235}\text{U} > ^{206}\text{Pb}/^{238}\text{U}$, suggestive of Pb loss during
179 subsequent tectonothermal events. Four grains have significantly older U-Pb ages than the
180 remaining analyses with the $^{207}\text{Pb}/^{206}\text{Pb}$ apparent ages of 2740 Ma, 2087 Ma, 1146 Ma and
181 1150 Ma (Table 1), and are interpreted as xenocrysts. Ten spots yield a $^{206}\text{Pb}/^{238}\text{U}$ weighted
182 mean age of 814 ± 12 Ma with MSWD = 1.01 (Fig. 4c), representing the formation age of
183 the sample.

184

185 **4.2. Geochemical characteristics**

186 Based on the mineral assemblage and geochemical characteristics, the amphibolites
187 from Jinping and Yuanyang are divided into two groups, referred to as Group 1 and Group 2.

188 Group 2 samples have higher FeOt, TiO₂ and P₂O₅ contents and lower CaO contents than
189 Group 1 (Table 2 and Fig. 5). Ni contents of Group 2 are relatively higher (100 to 130 ppm)
190 compared to the values of 10-22 ppm for Group 1. On the plot of Zr/TiO₂ versus Nb/Y,
191 Group 1 falls in the subalkaline field, whereas Group 2 samples plot in the alkaline field
192 (Table 2 and Fig. 6a). Group 1 has mg-number of 71~76, La/Yb of 7.2~7.7, TiO₂ of
193 0.37~0.76 wt. % and Nb of 3.19~ 5.22 ppm (Figs. 6b and 7). Group 2 samples, are
194 characterized by mg-number of 52~68 and La/Yb of 9.1~10.5 (Fig. 6b) with TiO₂ contents
195 ranging from 1.67 wt. % to 2.22 wt. % and Nb contents from 14.28 ppm to 18.43 ppm.

196 On REE-normalized plot, Group 1 has (La/Yb)cn of 4.98~5.91 and (Gd/Yb)cn of
197 1.60~1.65, and negative europium anomalies with δEu (2*Eu/(Sm+Gd) of 0.58~ 0.74 (Fig.
198 7a). Group 2 has a steeper REE-normalized pattern with higher LREEs contents, (La/Yb)cn
199 (6.55~7.52), (Gd/Yb)cn (1.90~2.23) and δEu (0.97~1.01) ratios than Group 1 (Fig. 7c). On
200 multi-element primitive mantle-normalized plot, Group 1 samples are characterized by
201 negative Nb-Ta ((Nb/La)n = 0.22~0.34) and P-Ti anomalies and positive Sr anomalies.
202 Group 2 has (Nb/La)n ratios ranging from 0.73 to 0.81, (Th/La)n ratios from 0.88 to 1.12
203 and (Hf/Sm)n from 0.93 to 1.02, and is marked by enrichment in LILEs and weak depletion
204 in Nb-Ta and Ti (Fig. 7b, d).

205 The initial Sr–Nd isotopic compositions for groups 1 and 2 are calculated back to their
206 formation age of ~800 Ma and ~810 Ma, respectively (Fig. 8b and Table 3). ⁸⁷Sr/⁸⁶Sr(t)
207 ratios for Group 1 range from 0.70493-0.70663 and have ε_{Nd}(t) values of -3.45 ~ -2.04. In
208 contrast, Group 2 display distinct Sr-Nd isotopic compositions with ⁸⁷Sr/⁸⁶Sr(t) ratios
209 ranging from 0.71040 to 0.70654 and ε_{Nd}(t) values from +4.08 to +4.39.

210

211 **5. Discussion**212 **5.1. Alteration effects**

213 Groups 1 and 2 samples have experienced greenschist to amphibolite facies
214 metamorphism. They show low loss on ignition (LOI) of less than 2.2 wt%. High field
215 strength elements (e.g., Th, Zr, Hf, Nb, Ta, Ti, Y and REE) and Nd isotopic compositions
216 are generally considered to be immobile during alteration or weathering (e.g., Barnes et al.,
217 1985; Wang et al., 2007a) and Zr is often used as a reference phase to test the mobility of
218 other incompatible elements (Rolland et al., 2009). Our samples show positive correlation
219 between Zr and Nb, Th, La, Yb, Nd, Sm and Ti for groups 1 and 2, whereas LOI shows little
220 or no correlation with Nb/La and Th/La ratios and $\epsilon_{\text{Nd}}(t)$ values (not shown). These
221 signatures, together with the subparallel REE and multi-element patterns in Figs. 7a-d,
222 suggest that the behavior of these elements can be used to trace the primary magmatic
223 features. Furthermore, the linear correlations on the Harker variation diagrams (Fig. 5) also
224 display insignificant effects of alteration.

225

226 **5.2. Petrogenesis of the Ailaoshan amphibolite**

227 The positive correlation between Al_2O_3 and SiO_2 but negative correlation between CaO
228 and SiO_2 of the Group 1 samples suggest a source characterized by low Al_2O_3 and high CaO
229 (Upton and Emeleus, 1987). Such signatures, combined with MgO of 8.82 to 12.07 wt %,
230 $\text{P}_2\text{O}_5/\text{Al}_2\text{O}_3$ of 0.002–0.004 and Gd/Yb of 1.9–2.0 (Table 2), are most likely inherited from a
231 garnet-bearing, orthopyroxene-rich source that had previously experienced melt extraction

232 (e.g., Hirose, 1997; Wang et al., 2007c, 2013a). Group 1 samples show enrichment in LILEs
233 and depletion in HFSEs with pronounced negative Nb-Ta and Zr-Hf anomalies (Fig. 7b).
234 These signatures, together with high Th/Yb (0.66–0.90), Ba/Nb, Zr/Nb, Sr/La and Th/Ce
235 ratios and low Nb/La, Ta/La and Ce/Pb ratios, indicate the similarity to typical
236 supra-subduction zone arc magmatic rocks and distinction from rocks in intraplate settings
237 (Fig. 9c, e.g., Pearce, 2008; Luhr and Haldar, 2006; Pearce and Peate, 1995). The
238 REE-normalized and multi-element primitive mantle normalized patterns of Group 1 are
239 also identical to the Barren Arc volcanic rocks and Neoproterozoic Panzhihua mafic rocks
240 (Fig. 7a and 7c).

241 Group 1 samples have negative $\epsilon_{\text{Nd}}(t)$ values of $-2.04 \sim -3.45$ (Table 3 and Fig. 8b),
242 indicate the involvement of crustal components rather than the addition of new slab-derived
243 fluid/melt within the magma source region (e.g., Wang et al., 2004, 2007c, 2013b). Possible
244 sources for crustal involvement include arc basement or the subduction-derived sediments.
245 Our modeling calculation suggests that ~10–30 % SCC crustal materials are required to
246 achieve the observed Nd isotopic composition of the Group 1 samples (Figs. 8a-d. e.g.,
247 Chen and Jahn, 1998; Wang et al., 2007c, 2011, 2012b). Such a large volume of crustal
248 materials in the mantle source is inconsistent with the Sr-Nd isotopic compositions and the
249 ratios of incompatible elements, and also fails to explain the major oxide characteristics of
250 the Group 1 samples. As a result, an alternative model for the petrogenesis of the Group 1
251 samples is proposed involving recent or ancient metasomatism of subduction-derived
252 sedimentary components. Such a petrogenesis can reasonably explain the geochemical
253 signature of the Group 1 samples, such as the correlations between Nb/Y, Rb/Y, Nb/Zr,

254 Th/Zr, Nb/U, Th/Nb, Ba/Nb and $\epsilon_{\text{Nd}}(t)$ (Figs. 11a, c, d; e.g., Fan et al., 2010; Kepezhinskas
255 et al., 1997; Pearce and Stern, 2006; Zhao and Zhou, 2007).

256 Group 2 shows lower Al_2O_3 , K_2O and CaO and higher $\text{P}_2\text{O}_5/\text{Al}_2\text{O}_3$ (0.019-0.020),
257 Nb/Ta (13.8-15.2), Ce/Y (2.04-2.15), Sm/Yb (2.4-2.9) and Gd/Yb (2.3-2.7) in comparison
258 with Group 1 (Table 1 and Figs. 5a-h). These features indicate a derivation from a mantle
259 source more enriched in garnet and which has undergone little or no depletion by a previous
260 melt extraction event (e.g., Class et al., 2000). The Nb/U values for Group 2 are markedly
261 lower than those of the average ocean island basalts (Fig. 6c). On the Gd/Yb versus Nb/La
262 discrimination diagram (Fig. 9a), Group 2 samples have higher Nb contents than typical arc
263 volcanic rocks, and can be classified as Nb-enriched basalt (e.g., Sajona et al., 1993, 1996).
264 Their compositions are similar to the Mindamao (Philippines) Nb-enriched island arc basalts
265 and the early Neoproterozoic Wuyi-Yunkai Nb-enriched arc basalt from the SCC (e.g.,
266 Wang et al., 2013a; Zhang et al., 2012a). Three petrogenetic models have been proposed for
267 Nb-enriched basalt involving (i) an OIB-like plume-related source, (ii) shallow-level crustal
268 assimilation en route, and (iii) a mantle wedge metasomatised by young slab-derived
269 components (e.g., Sajona et al., 1996; Kepezhinskas et al., 1996; Stern, 2002; Wang et al.,
270 2013a). Neoproterozoic OIB-derived mafic rocks have not been observed in the study area
271 and the geochemical characteristics of the Group 2 samples are distinct from those of OIB,
272 ruling out a plume-related origin. Group 2 has higher FeOt , TiO_2 and P_2O_5 contents and
273 lower CaO contents and is marked by enrichment in LILEs and insignificant in Nb-Ta and
274 Ti (Fig. 7b, d), precluding the possibility of the significant shallow-level crustal assimilation.
275 These samples show higher La/Yb , Th/Ce and Th/Nb ratios than average MORB (Sun and

276 McDonough, 1989). Their Nb/Ta ratios range from 13.8 to 15.2, (Ta/La)n ratios from 0.90
277 to 0.96, and (Hf/Sm)n from 0.93 to 1.02. These signatures argue for the involvement of
278 slab-derived melts in the Group 2 source. This is similar to those of Mindamao and
279 Wuyi-Yunkai Nb-enriched basalts that are interpreted as the product of interaction of subarc
280 mantle peridotite with siliceous slab-derived melt (Fig. 11b; e.g., Kepezhinskis et al., 1996,
281 1997; Wang et al. 2013a). The modification of a subduction- component in the Group 2
282 source is further evidenced by the correlations between Nb/Zr, Th/Zr, Nb/U, Th/Nb, Ba/Nb
283 and ϵ_{Nd} (Figs. 11a-d). Group 1 has arc-like signatures, and plots above the MORB array in
284 Fig. 9b (Pearce and Stern, 2006), similar to those of arc magma along the western and
285 northern margins of the Yangtze Block. The majority of the Group 2 samples plot between
286 MORB and western Yangtze arc magma, suggestive of the capture of subduction
287 components within the magma source, identical to the Scotia back-arc basin basalt (BABB)
288 whose source was modified by the South Sandwich arc (Fig. 9b; Pearce and Stern, 2006).

289

290 **5.3. Tectonic implications: ~815~800 Ma arc system along the SW Yangtze Block**

291 Our age data for amphibolites along the Ailaoshan zone give zircon U-Pb ages of $803 \pm$
292 7 Ma (Group 1), 813 ± 11 Ma (Group 2) and 814 ± 12 Ma (Group 2). Recent data for
293 orthogneiss within the Ailaoshan zone having U-Pb zircons ages ranging from 843 Ma to
294 803 Ma (e.g., Li, 2010; Liu et al., 2008a). These geochronological data indicate the presence
295 for the Neoproterozoic igneous rocks adjacent to the SW margin of the Yangtze Block.
296 Group 1 amphibolites display an affinity to arc volcanic rocks (Fig. 6c, Fig. 9a-c and Fig.
297 10a). Group 2 samples show higher HFSEs and Nb contents and lower Ti/Zr, V/Ti and Sc/Y

298 ratios than Group 1. On the plots of V versus Ti/1000, FeO*/MgO versus TiO₂ and Ti/Zr
299 versus V/Ti (e.g., Woodhead et al., 1993; Fan et al., 2004), Group 2 samples generally plot
300 in the field of BABB, similar to the East Scotia, North Fiji, Lau basin, Havre Trough and
301 East Woodlark lavas (e.g., Hollings and Kerrich, 2004; Macdonald et al., 2000).
302 Intra-oceanic BABB (e.g., South Sandwich Islands and Tonga-Kermadec arcs) is
303 geochemically indistinguishable from an N-MORB source (e.g., Hawkins, 1995) and has
304 (La/Yb)n < 2, Nb/La < 0.6 and Sm/Nd > 0.3. In contrast, the BABB with continental
305 basement usually exhibits E-MORB-like elemental and isotopic compositions with
306 (La/Yb)n > 3, Nb/La > 0.6 and Sm/Nd < 0.3 (e.g., Shinjo et al., 1999). Group 2 has elevated
307 LILEs, LREEs and HFSEs, and relatively low (Th/La)n. Their (La/Yb)n ratios range from
308 6.55 to 7.52, Nb/La from 0.76 to 0.84, Sm/Nd from 0.20 to 0.21, and Zr/Y from 5.87 to 6.69,
309 similar to those observed in Northern Okinawa Trough (Japan Sea) intra-continental BABB
310 (e.g., Gribble et al., 1998; Sandeman et al., 2006). In plots of Ce versus Yb and Ce/Nb
311 versus Th/Nb (Figs. 10b-d; Hawkesworth et al., 1993; Pearce, 1983), Group 2 samples plot
312 near the field of the Okinawa BABB and resemble continental margin arc basalts from
313 Philippines. The presence of the inherited zircons in 10HH-67A (e.g., 10HH-67A-02, -10,
314 -19 and -24) also points to the involvement of continental basement. As a result, it is herein
315 proposed that Group 1 samples formed in a magmatic arc environment and Group 2 in an
316 intra-continental BAB setting. Lu (1989) also suggested, on the basis of the voluminous
317 volcano-sedimentary associations and relatively uniform volcanic sequences in the
318 Ailaoshan Group/Complex, the development of a Neoproterozoic arc-back-arc setting along
319 the Ailaoshan zone.

320 The Neoproterozoic successions are fault-bounded both with respect to each other and
321 with respect to the bounding Yangtze and Indochina blocks. Comparison of the
322 geochronological and geochemical data from the Ailaoshan zone with those in the bounding
323 blocks favors the correlation with the western margin of the Yangtze Block. The temporal
324 equivalence of the two groups of amphibolite suggests that they originally formed in spatial
325 proximity as part of an overall coherent supra-subduction zone tectonic assemblage.
326 Furthermore, Neoproterozoic units have recently been recognized within the Ailaoshan
327 suture to the southwest of the study area (Figs. 1 and 12), with gabbro and granodiorite
328 yielding U-Pb zircon ages of 769 ± 7 Ma and 761 ± 11 Ma and their geochemical
329 composition suggesting a magmatic arc setting (e.g., Qi et al., 2012). Additionally, in the
330 PoSen complex in northern Vietnam, which is inferred to lie along a further extension of the
331 Ailaoshan suture zone (Hieu et al., 2009, 2012), the granitic rocks were dated at 760-751
332 Ma and show subduction-related geochemical signatures (Figs. 1 and 12 and Supplementary
333 table 1; e.g., Hieu et al., 2009, 2012; Lin et al., 2012; Liu et al., 2012; Wang et al., 2011a).
334 The synthesis of all data suggests an overall age-range of the Neoproterozoic igneous
335 activity within the Ailaoshan suture zone from at least 815 Ma to 750 Ma. This falls within
336 the overall age-range (860-730 Ma) of supra-subduction activity along the western margin
337 of the Yangtze Block (e.g., Zhao and Cawood, 2012; Zhao et al., 2011; Zhao and Zhou,
338 2007; Zhou et al., 2002a, b, 2006a, b). This contrasts with the time (~1000-820 Ma) of the
339 subduction-related magmatic activity along the Wuyi-Yunkai, Shuangxiwu and Jiangnan
340 Orogenes in the eastern and central parts of the SCC (Fig. 1; e.g., Cawood et al., 2013; Shu et
341 al., 2008, 2011; Wang et al., 2013b; Zhang et al., 2012a, b, 2013b). If the Neoproterozoic

342 igneous rocks within the Ailaoshan suture zone represent the disrupted southward extension
343 of the subduction-related rocks along the western margin of the Yangtze Block, then their
344 current disposition requires at least 400 km of left-lateral strike slip displacement along the
345 suture and the younger Cenozoic faults (e.g., Leloup et al., 1995; Tapponnier et al., 1990).

346 The arc and back-arc affinities of the Neoproterozoic igneous rocks along the
347 Ailaoshan suture zone (Figs. 7, 9 and 10a; Qi et al., 2012; Wang et al., 2011a) are consistent
348 with the supra-subduction setting inferred for the similar age igneous activity within the
349 SCC (Figs. 1 and 11; Cawood et al., 2013; Wang et al., 2013b; Zhou et al., 2002a, b). Our
350 samples show no evidence for plume or within-plate geochemical affinities, further
351 suggesting that the convergent plate margin activity took place with an accretionary setting
352 on the margin of Rodinia rather than in the intracratonic position (e.g., Cawood et al., 2008,
353 2009, 2010, 2013; Wang et al., 2013b).

354

355 **Acknowledgements** We would like to thank X-P Xia, T-P Peng, F-F Zhang and A-M Zhang
356 for their help during fieldwork and dating analyses. We are grateful to Prof Guochun Zhao
357 and two anonymous reviewers for their critical and constructive review on this paper. This
358 study was supported by China Natural Science Foundation (41190073 and 41372198),
359 National Basic Research Program of China (2014CB440901) and Natural Environment
360 Research Council (grant NE/J021822/1).

361 **References**

362 Bao, Z.W., Wang, Q., Bai, G.D., Zhao, Z.H., Song, Y.W., Liu, X.M., 2008. Geochronology and
363 geochemistry of the Fangcheng Neoproterozoic alkali-syenites in East Qinling orogen and its

- 364 geodynamic implications. Chinese Science Bulletin 53, 2050-2061.
- 365 Barnes, S.J., Naldrett, A.J., Gorton, M.P., 1985. The origin of the fractionation of platinum-group
366 elements in Terrestrial magmas. Chemical Geology 53, 303-323.
- 367 Cawood, P.A., Korsch, R.J., 2008. Assembling Australia: Proterozoic building of a continent.
368 Precambrian Research 166, 1-35.
- 369 Cawood, P.A., Kröner, A., Collins, W.J., Kusky, T.M., Mooney, W.D., Windley, B.F., 2009.
370 Accretionary orogens through Earth history, in Cawood, P.A., and Kröner, A., eds., Earth
371 accretionary systems in space and time. Geological Society of London Special Publication 318, p.
372 1-36.
- 373 Cawood, P.A., Strachan, R., Cutts, K., Kinny, P.D., Hand, M., Pisarevsky, S., 2010. Neoproterozoic
374 orogeny along the margin of Rodinia: Valhalla orogen, North Atlantic. Geology, 38(2), 99-102.
- 375 Cawood, P.A., Wang, Y.J., Xu, Y.J., Zhao, G.C., 2013. Locating South China in Rodinia and Gondwana:
376 a fragment of greater India lithosphere? Geology, 41(8), 903-906.
- 377 Charvet, J., Shu, L.S., Shi, Y.S., Guo, L.Z., Faure, M., 1996. The building of south China: collision of
378 Yangzi and Cathaysia blocks, problems and tentative answers. Journal of Southeast Asian Earth
379 Sciences 13, 223-235.
- 380 Chen, D.G., Deloule, E., Chen, H., Xiao, Q.K., Wu, Y.B., 2003. Preliminary study of microscale zircon
381 oxygen isotopes for Dabie-Sulu metamorphic rocks: ion probe in situ analyses. Chinese Science
382 Bulletin 48(16), 1670-1678.
- 383 Chen, J.F., Jahn, B.M., 1998. Crustal evolution of southeastern China: Nd and Sr isotopic evidence.
384 Tectonophysics 284, 101-133.
- 385 Chen, M., Zheng, J.P., Sun, M., Zhao, J.H., 2013. Mid-Neoproterozoic crustal evolution of the
386 northeastern Yangtze Block: evidence from the felsic-gneiss xenoliths hosted in the Donghai
387 Cenozoic basalts. Journal of Asian Earth Sciences 66, 108-122.
- 388 Chen, R.X., Zheng, Y.F., Xie, L.W., 2010. Metamorphic growth and recrystallization of zircon:
389 distinction by simultaneous in-situ analyses of trace elements, U-Th-Pb and Lu-Hf isotopes in zircons
390 from eclogite-facies rocks in the Sulu orogen. Lithos 114, 132-154.
- 391 Chen, R.X., Zheng, Y.F., Zhao, Z.F., Tang, J., Wu, F.Y., Liu, X.M., 2007. Zircon U-Pb age and Hf

- 392 isotope evidence for contrasting origin of bimodal protoliths for ultrahigh-pressure metamorphic
393 rocks from the Chinese Continental Scientific Drilling project. *Journal of Metamorphic Geology* 25,
394 873-894.
- 395 Class, C., Miller, D.M., Goldstein, S.L., Langmuir, C.H., 2000. Distinguishing melt and fluid subduction
396 components in Umnak Volcanics, Aleutian Arc. *Geochemistry Geophysics Geosystems* 1, 1004,
397 <http://dx.doi.org/10.1029/1999GC000010>.
- 398 Dong, Y.P., Liu, X.M., Santosh, M., Chen, Q., Zhang, X.N., Li, W., He, D.F., Zhang, G.W., 2012.
399 Neoproterozoic accretionary tectonics along the northwestern margin of the Yangtze Block, China:
400 constraints from zircon U-Pb geochronology and geochemistry. *Precambrian Research* 196, 247-274.
- 401 Dong, Y.P., Liu, X.M., Santosh, M., Zhang, X.N., Chen, Q., Yang, C., Yang, Z., 2011. Neoproterozoic
402 subduction tectonics of the northwestern Yangtze Block in South China: constraints from zircon U-Pb
403 geochronology and geochemistry of mafic intrusions in the Hannan Massif. *Precambrian Research*
404 189, 66-90.
- 405 Du, L.L., Geng, Y.S., Yang, C.H., Wang, X.S., Ren, L.D., Wang, Y.B., Yang, Z.S., 2007. New
406 understanding on Kangding Group on western margin of Yangtze Block: evidence from geochemistry
407 and chronology. *Acta Geologica Sinica* 81, 1562-1577 (in Chinese with English abstract).
- 408 Fan, W.M., Guo, F., Wang, Y.J., Zhang, M., 2004. Late Mesozoic volcanism in the northern Huaiyang
409 tectono-magmatic belt, central China: partial melts from a lithospheric mantle with subducted
410 continental crust relicts beneath the Dabie orogen? *Chemical Geology* 209, 27-48.
- 411 Fan, W.M., Wang, Y.J., Zhang, A.M., Zhang, F.F., Zhang, Y.Z., 2010. Permian arc-back-arc basin
412 development along the Ailaoshan tectonic zone: geochemical, isotopic and geochronological
413 evidence from the Mojiang volcanic rocks, Southwest China. *Lithos* 119, 553-568.
- 414 Ge, W.C., Li, X.H., Li, Z.X., Zhou, H.W., 2001. Mafic intrusions in Longsheng area: age and its
415 geological implications. *Chinese Journal of Geology* 36, 112-118 (in Chinese with English abstract).
- 416 Gribble, R.F., Stern, R.J., Newman, S., Bloomer, S.H., O'Hearn, T., 1998. Chemical and isotopic
417 composition of lavas from the Northern Mariana Trough: implications for magmagenesis in back-arc
418 basins. *Journal of Petrology* 39, 125-154.
- 419 Hacker, B.R., Wallis, S.R., Ratschbacher, L., Grove, M., Gehrels, G., 2006. High-temperature
420 geochronology constraints on the tectonic history and architecture of the ultrahigh-pressure
421 Dabie-Sulu Orogen. *Tectonics* 25, TC5006, doi:10.1029/2005TC001937.

- 422 Hawkesworth, C.J., Gallagher, K., Hergt, J.M., McDermott, F., 1993. Mantle and slab contributions in arc
 423 magmas. *Annual Review of Earth and Planetary Sciences* 21, 175-204.
- 424 Hawkins, J.W., 1995. The geology of the Lau Basin. In: Taylor, B. (Ed.), *Back-arc Basins: Tectonics and*
 425 *Magmatism*. Plenum Press, New York, pp. 63-138.
- 426 Hirose, K., 1997. Melting experiments on Iherzolite KLB-1 under hydrous conditions and generation of
 427 high-magnesian andesitic melts. *Geology* 25, 42-44.
- 428 Hieu, P.T., Chen, F., Zhu, X.Y., Wang, W., Nguyen, T.B.T., Bui, M.T., Nguyen, Q.L., 2009. Zircon
 429 U-Pb ages and Hf isotopic composition of the Posen granite in northwestern Vietnam. *Acta*
 430 *Petrologica Sinica* 25, 3141–3152 (in Chinese with English abstract).
- 431 Hieu, P.T., Chen F., Me L.T., Nguyen T.B.T., Siebel W., Lan T.G., 2012. Zircon U-Pb ages and Hf
 432 isotopic compositions from the Sin Quyen Formation: the Precambrian crustal evolution of northwest
 433 Vietnam. *International Geology Review* 54, 1548-1561.
- 434 Hollings, P., Kerrich, R., 2004. Geochemical systematics of tholeiites from the 2.86 Ga Pickle Crow
 435 Assemblage, northwestern Ontario: arc basalts with positive and negative Nb-Hf anomalies.
 436 *Precambrian Research* 134, 1-20.
- 437 Hu, J., Qiu, J.S., Wang, R.C., Jiang, S.Y., Yu, J.H., Ni, P., 2007. Earliest response of the Neoproterozoic
 438 Rodinia break-up in the northeastern Yangtze craton: constraints from zircon U-Pb geochronology
 439 and Nd isotopes of the gneissic alkaline granites in Donghai area. *Acta Petrologica Sinica* 23,
 440 1321-1333 (in Chinese with English Abstract).
- 441 Huang, X.L., Xu, Y.G., Li, X.H., Li, W.X., Lan, J.B., Zhang, H.H., Liu, Y.S., Wang, Y.B., Li, H.Y., Luo,
 442 Z.Y., Yang, Q.J., 2008. Petrogenesis and tectonic implications of Neoproterozoic, highly fractionated
 443 A-type granites from Mianning, South China. *Precambrian Research* 165, 190-204.
- 444 Kepezhinskis, P., Defant, M.J., Drummond, M.S., 1996. Progressive enrichment of island arc mantle by
 445 melt-peridotite interaction inferred from Kamchatka xenoliths. *Geochimica Et Cosmochimica Acta*
 446 60, 1217-1229.
- 447 Kepezhinskis, P., McDermott, F., Defant, M.J., Hochstaedter, A., Drummond, M.S., Hawkesworth, C.J.,
 448 Koloskov, A., Maury, R.C., Bellon, H., 1997. Trace element and Sr-Nd-Pb isotopic constraints on a
 449 three-component model of Kamchatka arc petrogenesis. *Geochimica Et Cosmochimica Acta* 61,
 450 577-600.
- 451 Leat, P.T., Livermore, R.A., Millar, I.L., Pearce, J.A., 2000. Magma supply in back-arc spreading centre

- 452 segment e2, east Scotia Ridge. *Journal of Petrology* 41, 845-866.
- 453 Leloup, P.H., Lacassin, R., Tapponnier, P., Scharer, U., Zhong, D.L., Liu, X.H., Zhang, L.S., Ji, S.C.,
454 Trinh, P.T., 1995. The Ailao Shan-Red River shear zone (Yunnan, China), Tertiary transform
455 boundary of Indochina. *Tectonophysics* 251, 3-10.
- 456 Li, B.L., 2010. Thermal evolutional history and geochronological constrains on metamorphic-
457 deformational zones in west Yunnan Province. Dissertation for Doctoral Degree, pp.57-59.
- 458 Li, W.X., Li, X.H., Li, Z.X., 2008b. Middle Neoproterozoic syn-rifting volcanic rocks in Guangfeng,
459 South China: petrogenesis and tectonic significance. *Geological Magazine* 145, 475-489.
- 460 Li, W.X., Li, X.H., Li, Z.X., 2010. Ca. 850 Ma bimodal volcanic rocks in northeastern Jiangxi Province,
461 South China: initial extension during the breakup of Rodinia? *American Journal of Science* 310,
462 951-980.
- 463 Li, X.H., 1999. U-Pb zircon ages of granites from the southern margin of the Yangtze Block: timing of
464 Neoproterozoic Jinning orogeny in SE China and implications for Rodinia Assembly. *Precambrian
465 Research* 97, 43-57.
- 466 Li, X.H., Li, W.X., Li, Z.X., Liu, Y., 2008a. 850-790 Ma bimodal volcanic and intrusive rocks in
467 northern Zhejiang, South China: a major episode of continental rift magmatism during the breakup of
468 Rodinia. *Lithos* 102, 341-357.
- 469 Li, X.H., Li, W.X., Li, Z.X., Lo, C.H., Wang, J., Ye, M.F., Yang, Y.H., 2009b. Amalgamation between
470 the Yangtze and Cathaysia Blocks in South China: constraints from SHRIMP U-Pb zircon ages,
471 geochemistry and Nd-Hf isotopes of the Shuangxiwu volcanic rocks. *Precambrian Research* 174,
472 117-128.
- 473 Li, X.H., Li, Z.X., Ge, W.C., Zhou, H.W., Li, W.X., Liu, Y., Wingate, M.T.D., 2003b. Neoproterozoic
474 granitoids in South China: crustal melting above a mantle plume at ca. 825 Ma? *Precambrian
475 Research* 122, 45-83.
- 476 Li, X.H., Li, Z.X., Sinclair, J.A., Li, W.X., Carter, G., 2006. Revisiting the “Yanbian Terrane”:
477 implications for Neoproterozoic tectonic evolution of the western Yangtze Block, South China.
478 *Precambrian Research* 151, 14-30.
- 479 Li, X.H., Li, Z.X., Zhou, H.W., Liu, Y., Kinny, P.D., 2002. U-Pb zircon geochronology, geochemistry
480 and Nd isotopic study of Neoproterozoic bimodal volcanic rocks in the Kangdian Rift of South China:
481 implications for the initial rifting of Rodinia. *Precambrian Research* 113, 135-154.

- 482 Li, X.H., Li, Z.X., Zhou, H.W., Liu, Y., Liang, X.R., Li, W.X., 2003c. SHRIMP U-Pb zircon age,
483 geochemistry and Nd isotope of the Guandaoshan pluton in SW Sichuan: petrogenesis and tectonic
484 significance. *Science in China Series D: Earth Sciences* 46, 73-83.
- 485 Li, X.H., Liu, Y., Li, Q.L., Guo, C.H., Chamberlain, K.R., 2009a. Precise determination of Phanerozoic
486 zircon Pb/Pb age by multicollector SIMS without external standardization (vol 10, Q04010, 2009).
487 *Geochemistry Geophysics Geosystems* 10.
- 488 Li, Z.X., Li, X.H., Kinny, P.D., Wang, J., Zhang, S., Zhou, H., 2003a. Geochronology of Neoproterozoic
489 syn-rift magmatism in the Yangtze Craton, South China and correlations with other continents:
490 evidence for a mantle superplume that broke up Rodinia. *Precambrian Research* 122, 85-109.
- 491 Li, Z.X., Zhang, L.H., Powell, C.M., 1995. South China in Rodinia: part of the missing link between
492 Australia-East Antarctica and Laurentia? *Geology* 23(5), 407-410.
- 493 Liang, X.R., Wei, G.J., Li, X.H., Liu, Y., 2003. Precise measurement of $^{143}\text{Nd}/^{144}\text{Nd}$ and Sm/Nd ratios
494 using multiple-collectors inductively coupled plasma-mass spectrometer (MC-ICPMS). *Geochimica*
495 32, 91-96 (in Chinese with English abstract).
- 496 Lin, T.H., Chung, S.L., Chiu, H.Y., Wu, F.Y., Yeh, M.W., Searle, M.P., Iizuka, Y., 2012. Zircon U-Pb
497 and Hf isotope constraints from the Ailao Shan-Red River shear zone on the tectonic and crustal
498 evolution of southwestern China. *Chemical Geology* 291, 23-37.
- 499 Ling, H.F., Shen, W.Z., Wang, R.C., Xu, S.J., 2001. Geochemical characteristics and genesis of
500 Neoproterozoic granitoids in the northwestern margin of the Yangtze Block. *Physics and Chemistry*
501 of the Earth Part a: Solid Earth and Geodesy 26, 805-819.
- 502 Ling, W.L., Gao, S., Zhang, B.R., Li, H.M., Liu, Y., Cheng, J.P., 2003. Neoproterozoic tectonic
503 evolution of the northwestern Yangtze craton, South China: implications for amalgamation and
504 break-up of the Rodinia Supercontinent. *Precambrian Research* 122, 111-140.
- 505 Liu, F., Wang, F., Liu, P., Liu, C., 2012. Multiple metamorphic events revealed by zircons from the
506 Diancang Shan-Ailao Shan metamorphic complex, southeastern Tibetan Plateau. *Gondwana*
507 *Research*. <http://dx.doi.org/10.1016/j.gr.2012.10.016>.
- 508 Liu, F.L., Gerdes, A., Zeng, L.S., Xue, H.M., 2008b. SHRIMP U-Pb dating, trace elements and the Lu-Hf
509 isotope system of coesite-bearing zircon from amphibolite in the SW Sulu UHP terrane, eastern
510 China. *Geochimica Et Cosmochimica Acta* 72, 2973-3000.
- 511 Liu, F.L., Xu, Z.Q., Yang, J.S., Zhang, Z.M., Xue, H.M., Li, T.F., 2004. Geochemical characteristics and

- 512 UHP metamorphism of granitic gneisses in the main drilling hole of Chinese Continental Scientific
513 Drilling Project and its adjacent area. *Acta Petrologica Sinica* 20, 9-26 (in Chinese with English
514 Abstract).
- 515 Liu, J.B., Zhang, L.M., 2013. Neoproterozoic low to negative $\delta^{18}\text{O}$ volcanic and intrusive rocks in the
516 Qinling Mountains and their geological significance. *Precambrian Research*, 230(0), 138-167.
- 517 Liu, J.L., Wang, A.J., Cao, S.Y., Zou, Y.X., Tang, Y., Chen, Y., 2008a. Geochronology and tectonic
518 implication of migmatites from Diancangshan, western Yunnan, China. *Acta Petrologica Sinica* 24,
519 413-420 (in Chinese with English abstract).
- 520 Lu, L.Z., 1989. The metamorphic series and crustal evolution of the basement of the Yangtze platform.
521 *Journal of Southeast Asian Earth Sciences* 3, 293-301.
- 522 Ludwig, K.R., 2001. Users manual for Isoplot/Ex rev. 2.49. Berkeley Geochronology Centre Special
523 Publication, pp. 56.
- 524 Luhr, J.F., Haldar, D., 2006. Barren Island Volcano (NE Indian Ocean): island-arc high-alumina basalts
525 produced by troctolite contamination. *Journal of Volcanology and Geothermal Research* 149,
526 177-212.
- 527 Ma, G., Li, H., Zhang, Z., 1984. An investigation of the age limits of the Sinian System in South China.
528 *Bull. Yichang Institute of Geology Mineral Research* 8, 1-29 (in Chinese with English Abstract).
- 529 Ma, G., Zhang, Z., Li, H., Chen, P., Huang, Z., 1989. A geochronostratigraphical study of the Sinian
530 System in Yangtze Platform. *Bull. Yichang Institute of Geology Mineral Research* 14, 83-124 (in
531 Chinese with English Abstract).
- 532 Macdonald, R., Hawkesworth, C.J., Heath, E., 2000. The Lesser Antilles volcanic chain: a study in arc
533 magmatism. *Earth Science Reviews* 49, 1-76.
- 534 Pearce, J.A., 1983. In: Hawkesworth, C.J., Norry, M.J. (Eds.), *Continental basalts and mantle xenolith*
535 (*Shaiva Geology Series*). Shiva, pp. 230-249.
- 536 Pearce, J.A., 2008. Geochemical fingerprinting of oceanic basalts with applications to ophiolite
537 classification and the search for Archean oceanic crust. *Lithos* 100, 14-48.
- 538 Pearce, J.A., Peate, D.W., 1995. Tectonic implications of the composition of volcanic arc magmas.
539 *Annual Review of Earth and Planetary Sciences* 23, 251-285.
- 540 Pearce, J.A., Stern, R.J., 2006. The origin of back-arc basin magmas: trace element and isotope
541 perspectives. *AGU Geophysical Monograph Series* 166, 63-86.

- 542 Pei, X.Z., Li, Z.C., Ding, S.P., Li, R.B., Feng, J.Y., Sun, Y., Zhang, Y.F., Liu, Z.Q., 2009.
543 Neoproterozoic Jiaoziding peraluminous granite in the northwest margin of Yangtze Block: zircon
544 SHRIMP U-Pb age and geochemistry, and their tectonic significance. *Earth Science Frontiers* 16,
545 231-249 (in Chinese with English Abstract).
- 546 Qi, L., Jing, H., Gregoire, D.C., 2000. Determination of trace elements in granites by inductively coupled
547 plasma mass spectrometry. *Talanta* 51, 507-513.
- 548 Qi, X.X., Zeng, L.S., Zhu, L.H., Hu, Z.C., Hou, K.J., 2012. Zircon U-Pb and Lu-Hf isotopic systematics
549 of the Daping plutonic rocks: implications for the Neoproterozoic tectonic evolution of the
550 northeastern margin of the Indochina block, Southwest China. *Gondwana Research* 21, 180-193.
- 551 Qin, X.F., Pan, Y.M., Li, L., Li, R.S., Zhou, F.S., Hu, G.A., Zhong, F.Y., 2006. Zircon SHRIMP U-Pb
552 geochronology of the Yunkai metamorphic complex in southeastern Guangxi, China. *Geological
553 Bulletin of China* 25 (5), 553-559.
- 554 Qiu, Y.M., Gao, S., McNaughton, N.J., Groves, D.I., Ling, W.L., 2000. First evidence of >3.2 Ga
555 continental crust in the Yangtze Craton of South China and its implications for Archean crustal
556 evolution and Phanerozoic tectonics. *Geology* 28 (1), 11-14.
- 557 Roger, F., Calassou, S., 1997. U-Pb geochronology on zircon and isotope geochemistry (Pb, Sr and Nd)
558 of the basement in the Songpan-Garze fold belt (China). *Comptes Rendus De L Academie Des
559 Sciences Serie II Fascicule a-Sciences De La Terre Et Des Planetes* 324, 819-826.
- 560 Rolland, Y., Galoyan, G., Bosch, D., Sosson, M., Corsini, M., Fornari, M., Verati, C., 2009. Jurassic
561 back-arc and Cretaceous hot-spot series In the Armenian ophiolites: implications for the obduction
562 process. *Lithos* 112, 163-187.
- 563 Sajona, F.G., Maury, R.C., Bellon, H., Cotten, J., Defant, M., 1996. High field strength element
564 enrichment of Pliocene-Pleistocene Island arc basalts, Zamboanga Peninsula, western Mindanao
565 (Philippines). *Journal of Petrology* 37, 693-726.
- 566 Sajona, F.G., Maury, R.C., Bellon, H., Cotten, J., Defant, M.J., Pubellier, M., 1993. Initiation of
567 subduction and the generation of slab melts in western and eastern Mindanao, Philippines. *Geology*
568 21, 1007-1010.
- 569 Sandeman, H.A., Hanmer, S., Tella, S., Armitage, A.A., Davis, W.J., Ryan, J.J., 2006. Petrogenesis of
570 Neoarchaean volcanic rocks of the MacQuoid supracrustal belt: a back-arc setting for the
571 northwestern Hearne subdomain, western Churchill Province, Canada. *Precambrian Research* 144,

- 572 140-165.
- 573 Shinjo, R., Chung, S.L., Kato, Y., Kimura, M., 1999. Geochemical and Sr-Nd isotopic characteristics of
574 volcanic rocks from the Okinawa Trough and Ryukyu Arc: implications for the evolution of a young,
575 intracontinental back arc basin. *Journal of Geophysical Research: Solid Earth* 104, 10591-10608.
- 576 Shu, L.S., Deng, P., Yu, J.H., Wang, Y.B., Jiang, S.Y., 2008. The age and tectonic environment of the
577 rhyolitic rocks on the western side of Wuyi Mountain, South China. *Science in China Series D: Earth*
578 *Sciences* 51(8), 1053-1063.
- 579 Shu, L.S., Faure, M., Yu, J.H., Jahn, B.M., 2011. Geochronological and geochemical features of the
580 Cathaysia block (South China): new evidence for the Neoproterozoic breakup of Rodinia.
581 *Precambrian Research* 187(3-4), 263-276.
- 582 Sinclair, J.A., 2001. Petrology, geochemistry, and geochronology of the “Yanbian ophiolite suite”, South
583 China: implications for the western extension of the Sibao Orogen. Honours Thesis, The University
584 of Western Australia, Perth, pp. 69 (plus appendixes).
- 585 Stacey, J.S., Kramers, J.D., 1975. Approximation of terrestrial lead isotope evolution by a 2-stage model.
586 *Earth and Planetary Science Letters* 26, 207-221.
- 587 Stern, R. J., 2002. Subduction zones: *Reviews of Geophysics* 40, 4.
- 588 Sun, S.S., McDonough, W.F., 1989. Chemical and isotopic systematics of oceanic basalts: implications
589 for mantle composition and processes. *Geological Society, London, Special Publications* 42, 313-345.
- 590 Tapponnier, P., Lacassin, R., Leloup, P.H., Scharer, U., Zhong, D.L., Wu, H.W., Liu, X.H., Ji, S.C.,
591 Zhang, L.S., Zhong, J.Y., 1990. The Ailao Shan-Red River metamorphic belt: Tertiary left-lateral
592 shear between Indochina and South China. *Nature* 343, 431-437.
- 593 Upton, B.G.J., Emeleus, C.H., 1987. Mid-Proterozoic alkaline magmatism in southern Greenland: the
594 Gardar province. In: Fitton, J.G., Upton, B.G.J. (Eds.), *Alkaline Igneous Rocks* Geological Society
595 Special Publication 30, 449-471.
- 596 Viruete, J.E., Contreras, F., Stein, G., Urien, P., Joubert, M., Perez-Estaun, A., Friedman, R., Ullrich, T.,
597 2007. Magmatic relationships and ages between adakites, magnesian andesites and Nb-enriched
598 basalt-andesites from Hispaniola: record of a major change in the Caribbean island arc magma
599 sources. *Lithos* 99, 151-177.
- 600 Wang, P.L., Lo, C.H., Lan, C.Y., Chung, S.L., Lee, T.Y., Tran, N.N., Sano, Y., 2011a.
601 Thermochronology of the PoSen complex, northern Vietnam: implications for tectonic evolution in

- 602 SE Asia. Journal of Asian Earth Sciences 40, 1044-1055.
- 603 Wang, Q., Wyman, D.A., Li, Z.X., Bao, Z.W., Zhao, Z.H., Wang, Y.X., Jian, P., Yang, Y.H., Chen, L.L.,
604 2010. Petrology, geochronology and geochemistry of ca. 780 Ma A-type granites in South China:
605 petrogenesis and implications for crustal growth during the breakup of the supercontinent Rodinia.
606 Precambrian Research 178, 185-208.
- 607 Wang, X.C., Li, X.H., Li, W.X., Li, Z.X., 2007b. Ca. 825 Ma komatiitic basalts in South China: first
608 evidence for > 1500 degrees C mantle melts by a Rodinian mantle plume. Geology 35, 1103-1106.
- 609 Wang, X.C., Li, X.H., Li, W.X., Li, Z.X., Liu, Y., Yang, Y.H., Liang, X.R., Tu, X.L., 2008c. The Bikou
610 basalts in the northwestern Yangtze block, South China: remnants of 820-810 Ma continental flood
611 basalts? Geological Society of America Bulletin 120, 1478-1492.
- 612 Wang, X.L., Shu, L.S., Xing, G.F., Zhou, J.C., Tang, M., Shu, X.J., Qi, L., Hu, Y.H., 2012a.
613 Post-orogenic extension in the eastern part of the Jiangnan orogen: evidence from ca 800-760 Ma
614 volcanic rocks. Precambrian Research 222, 404-423.
- 615 Wang, X.L., Zhao, G.C., Zhou, J.C., Liu, Y.S., Hu, J., 2008a. Geochronology and Hf isotopes of zircon
616 from volcanic rocks of the Shuangqiaoshan Group, South China: implications for the Neoproterozoic
617 tectonic evolution of the eastern Jiangnan orogen. Gondwana Research 14, 355-367.
- 618 Wang, X.L., Zhou, J.C., Qi, J.S., Jiang, S.Y., Shi, Y.R., 2008b. Geochronology and geochemistry of
619 Neoproterozoic mafic rocks from western Hunan, South China: implications for petrogenesis and
620 post-orogenic extension. Geological Magazine 145, 215-233.
- 621 Wang, X.L., Zhou, J.C., Qiu, J.S., Zhang, W.L., Liu, X.M., Zhang, G.L., 2006. LA-ICP-MS U-Pb zircon
622 geochronology of the Neoproterozoic igneous rocks from Northern Guangxi, South China:
623 implications for tectonic evolution. Precambrian Research 145, 111-130.
- 624 Wang, Y.J., Fan, W.M., Zhao, G.C., Ji, S.C., Peng, T.P., 2007a. Zircon U-Pb geochronology of gneissic
625 rocks in the Yunkai massif and its implications on the Caledonian event in the South China Block.
626 Gondwana Research 12, 404-416.
- 627 Wang, Y.J., Fang, W.M., Zhang, Y.H., Guo, F., Zhang, H.F., Peng, T.P., 2004. Geochemical $^{40}\text{Ar}/^{39}\text{Ar}$
628 geochronological and Sr-Nd isotopic constraints on the origin of Paleoproterozoic mafic dikes from
629 the southern Taihang Mountains and implications for the ca. 1800 Ma event of the North China
630 Craton. Precambrian Research 135, 55-77.
- 631 Wang, Y.J., Wu, C.M., Zhang, A.M., Fan, W.M., Zhang, Y.H., Zhang, Y.Z., Peng, T.P., Yin, C.Q.,

- 632 2012b. Kwangssian and Indosinian reworking of the eastern South China Block: constraints on zircon
633 U-Pb geochronology and metamorphism of amphibolites and granulites. *Lithos* 150, 227-242.
- 634 Wang, Y.J., Zhang, A.M., Fan, W.M., Zhang, Y.H., Zhang, Y.Z., 2013a. Origin of paleosubduction-
635 modified mantle for Silurian gabbro in the Cathaysia Block: geochronological and geochemical
636 evidence. *Lithos* 160, 37-54.
- 637 Wang, Y. J., Zhang, A. M., Cawood, P. A., Fan, W. M., Xu, J. F., Zhang, G. W., Zhang, Y. Z., 2013b,
638 Geochronological, geochemical and Nd-Hf-Os isotopic fingerprinting of an early Neoproterozoic
639 arc-back-arc system in South China and its accretionary assembly along the margin of Rodinia.
640 *Precambrian Research* 231, 343-371.
- 641 Wang, Y.J., Zhang, A.M., Fan, W.M., Zhao, G.C., Zhang, G.W., Zhang, Y.Z., Zhang, F.F., Li, S.Z., 2011.
642 Kwangssian crustal anatexis within the eastern South China Block: geochemical, zircon U-Pb
643 geochronological and Hf isotopic fingerprints from the gneissoid granites of Wugong and
644 Wuyi-Yunkai Domains. *Lithos* 127, 239-260.
- 645 Wang, Y.J., Zhao, G.C., Fan, W.M., Peng, T.P., Sun, L.H., Xia, X.P., 2007c. LA-ICP-MS U-Pb zircon
646 geochronology and geochemistry of Paleoproterozoic mafic dykes from western Shandong Province:
647 implications for back-arc basin magmatism in the Eastern Block, North China Craton. *Precambrian*
648 *Research* 154, 107-124.
- 649 Wiedenbeck, M., Alle, P., Corfu, F., Griffin, W.L., Meier, M., Oberli, F., Vonquadt, A., Roddick, J.C.,
650 Speigel, W., 1995. 3 natural zircon standards for U-Th-Pb, Lu-Hf, trace-element and REE analyses.
651 *Geostandard Newslett* 19, 1-23.
- 652 Winchester, J.A., Floyd, P.A., 1977. Geochemical discrimination of different magma series and their
653 differentiation products using immobile elements. *Chemical Geology* 20, 325-343.
- 654 Woodhead, J., Eggins, S., Gamble, J., 1993. High-field strength and transition element systematics in
655 island-arc and back-arc basin basalts: evidence for multiphase melt extraction and a depleted mantle
656 wedge. *Earth and Planetary Science Letters* 114(4), 491-504.
- 657 Wu, G.G., Yu, X.Q., Di, Y.J., Zhang, D., 2010. Neoproterozoic tectonic setting of southeast China: new
658 constraints from SHRIMP U-Pb zircon ages and petrographic studies on the Mamianshan Group.
659 *Acta Geologica Sinica: English Edition* 84, 333-344.
- 660 Xia, L.Q., Xia, Z.C., Ma, Z.P., Xu, X.Y., Li, X.M., 2009. Petrogenesis of volcanic rocks from Xixiang
661 Group in middle part of South Qinling Mountains. *Northwestern Geology* 42, 1-37 (in Chinese with

- 662 English Abstract).
- 663 Xia, X.P., Sun, M., Zhao, G.C., Li, H.M., Zhou, M.F., 2004. Spot zircon U-Pb isotope analysis by
664 ICP-MS coupled with a frequency quintupled (213 nm) Nd-YAG laser system. *Geochemical Journal*
665 38, 191-200.
- 666 Xu, H., Yang, T., Liu, F., Liou, J.G., 2001. Multi age-time evolution of granite gneissesgranite in the
667 southern Sulu HP-UHP metamorphic belt. *Acta Geologica Sinica* 75, 371-378 (in Chinese with
668 English Abstract).
- 669 Xu, Z.Q., Liu, F.L., Qi, X.X., Zhang, Z.M., Yang, J.S., Zeng, L.S., Liang, F.H., 2006. Record for Rodinia
670 suppercontinent breakup event in the south Sulu ultra-high pressure metamorphic terrane. *Acta
671 Petrologica Sinica* 22, 1745-1760 (in Chinese with English Abstract).
- 672 Xue, H.M., Ma, F., Song, Y.Q., Xie, Y.P., 2010. Geochronology and geochemistry of the Neoproterozoic
673 granitoid association from eastern segment of the Jiangnan orogen, China: constraints on the timing
674 and process of amalgamation between the Yangtze and Cathaysia blocks. *Acta Petrologica Sinica* 26,
675 3215-3244 (in Chinese with English abstract).
- 676 Yan, Q.R., Hanson, A.D., Wang, Z.Q., Druschke, P.A., Yan, Z., Wang, T., Liu, D.Y., Song, B., Pan, P.,
677 Zhou, H., Jiang, C.F., 2004. Neoproterozoic subduction and rifting on the northern margin of the
678 Yangtze Plate, China: implications for Rodinia reconstruction. *International Geology Review* 46,
679 817-832.
- 680 Ye, M.F., Li, X.H., Li, W.X., Liu, Y., Li, Z.X., 2007. SHRIMP zircon U-Pb geochronological and
681 whole-rock geochemical evidence for an early Neoproterozoic Sibaoian magmatic arc along the
682 southeastern margin of the Yangtze Block. *Gondwana Research* 12, 144-156.
- 683 Yin, C. Q., Lin, S. F., Davis, D. W., Xing, G. F., Davis, W. J., Cheng, G. H., Xiao, W. J., Li, L. M., 2013.
684 Tectonic evolution of the southeastern margin of the Yangtze Block: constraints from SHRIMP U-Pb
685 and LA-ICP-MS Hf isotopic studies of zircon from the eastern Jiangnan Orogenic Belt and
686 implications for the tectonic interpretation of South China. *Precambrian Research* 236, 145-156.
- 687 Yunnan BGMR (Bureau of geology and mineral resources of Yunnan), 1983. *Geological Map of Yunnan*,
688 scale 1:1 000000. Kumming (in Chinese with English abstract).
- 689 Zeng, W., Zhou, H.W., Zhong, Z.Q., Zeng, Z.G., Li, H.M., 2005. Single zircon U-Pb ages and their
690 tectonic implications of Neoproterozoic magmatic rocks in southeastern Guizhou, China. *Geochimica*
691 34, 548-556 (in Chinese with English abstract).

- 692 Zhang, A.M., Wang, Y.J., Fan, W.M., Zhang, Y.Z., Yang, J., 2012a. Earliest Neoproterozoic (ca. 1.0 Ga)
693 arc-back-arc basin nature along the northern Yunkai Domain of the Cathaysia Block:
694 geochronological and geochemical evidence from the metabasite. *Precambrian Research* 220,
695 217-233.
- 696 Zhang, C.L., Li, H.K., Santosh, M., 2013b. Revisiting the tectonic evolution of South China: interaction
697 between the Rodinia superplume and plate subduction? *Terra Nova* 25, 212-220.
- 698 Zhang, C.L., Liu, L., Zhang, G.W., Wang, T., Chen, D.L., Yuan, H.L., Liu, X.M., Yan, Y.X., 2004.
699 Determination of Neoproterozoic post-collisional granites in the North Qinling Mountains and its
700 tectonic significance. *Earth Science Frontier* 11, 33-42 (in Chinese with English abstract).
- 701 Zhang, G.W., Yu, Z.P., Dong, Y.P., Yao, A.P., 2000. On Precambrian framework and evolution of the
702 Qinling belt. *Acta Petrologica Sinica* 16, 11-21.
- 703 Zhang, S.B., Wu, R.X., Zheng, Y.F., 2012c. Neoproterozoic continental accretion in South China:
704 geochemical evidence from the Fuchuan ophiolite in the Jiangnan orogen. *Precambrian Research* 220,
705 45-64.
- 706 Zhang, Y.Z., Wang, Y.J., Fan, W.M., Zhang, A.M., Ma, L.Y., 2012b. Geochronological and geochemical
707 constraints on the metasomatised source for the Neoproterozoic (similar to 825 Ma) high-mg volcanic
708 rocks from the Cangshuipu area (Hunan Province) along the Jiangnan domain and their tectonic
709 implications. *Precambrian Research* 220, 139-157.
- 710 Zhang, Y.Z., Wang, Y.J., Geng, H.Y., Zhang, Y.H., Fan, W.M., Zhong, H., 2013b. Early Neoproterozoic
711 (similar to 850 Ma) back-arc basin in the Central Jiangnan Orogen (Eastern South China):
712 geochronological and petrogenetic constraints from meta-basalts. *Precambrian Research* 231,
713 325-342.
- 714 Zhang, Z.Q., Zhang, G.W., Liu, D.Y., Wang, Z.Q., Tan, S.H., Wang, J.H., 2006. Isotopic
715 geochronology and geochemistry of ophiolites, granites and clastic sedimentary rocks in the
716 Qinling-Dabie Orogenic Belt. Geological Publishing House, Beijing (in Chinese).
- 717 Zhang, Z.L., Yuan, H.H., Nan, Y., 1998. Whole grain zircon evaporation for age of Luoyu formation,
718 Yunkai Group. *Mineralogy Petrology* 18, 85-90 (in Chinese with English abstract).
- 719 Zhao, F.Q., Zhao, W.P., Zuo, Y.C., Li, Z.H., Xue, K.Q., 2006. U-Pb geochronology of Neoproterozoic
720 magmatic rocks in Hanzhong, southern Shaanxi, China. *Geological Bulletin of China* 25, 383-388 (in
721 Chinese with English abstract).

- 722 Zhao, G.C., Cawood, P.A., 1999. Tectonothermal evolution of the Mayuan assemblage in the Cathaysia
723 Block: implications for Neoproterozoic collision-related assembly of the South China craton.
724 American Journal of Science 299, 309-339.
- 725 Zhao, G.C., Cawood, P.A., 2012. Precambrian geology of China. Precambrian Research 222, 13-54.
- 726 Zhao, G.C., Guo, J.H., 2012. Precambrian geology of China: preface. Precambrian Research 222, 1-12.
- 727 Zhao, J.H., Zhou, M.F., Yan, D.P., Zheng, J.P., Li, J.W., 2011. Reappraisal of the ages of Neoproterozoic
728 strata in South China: no connection with the Grenvillian orogeny. Geology 39, 299-302.
- 729 Zhao, J.H., Zhou, M.F., Zheng, J.P., 2013. Neoproterozoic high-K granites produced by melting of newly
730 formed mafic crust in the Huangling region, South China. Precambrian Research 233, 97-107.
- 731 Zhao, J.H., Zhou, M.F., 2007. Geochemistry of Neoproterozoic mafic intrusions in the Panzhihua district
732 (Sichuan Province, SW China): implications for subduction-related metasomatism in the upper
733 mantle. Precambrian Research 152, 27-47.
- 734 Zhao, J.H., Zhou, M.F., 2008. Neoproterozoic adakitic plutons in the northern margin of the Yangtze
735 Block, China: partial melting of a thickened lower crust and implications for secular crustal evolution.
736 Lithos 104, 231-248.
- 737 Zhao, J.H., Zhou, M.F., 2009. Secular evolution of the Neoproterozoic lithospheric mantle underneath the
738 northern margin of the Yangtze Block, South China. Lithos 107, 152-168.
- 739 Zhao, J.H., Zhou, M.F., Zheng, J.P., Fang, S.M., 2010. Neoproterozoic crustal growth and reworking of
740 the Northwestern Yangtze Block: constraints from the Xixiang dioritic intrusion, South China. Lithos
741 120, 439-452.
- 742 Zhao, X.F., Zhou, M.F., Li, J.W., Wu, F.Y., 2008. Association of Neoproterozoic A- and I-type granites
743 in South China: implications for generation of A-type granites in a subduction-related environment.
744 Chemical Geology 257, 1-15.
- 745 Zheng, Y.F., Wu, R.X., Wu, Y.B., Zhang, S.B., Yuan, H.L., Wu, F.Y., 2008. Rift melting of juvenile
746 arc-derived crust: geochemical evidence from Neoproterozoic volcanic and granitic rocks in the
747 Jiangnan Orogen, South China. Precambrian Research 163, 351-383.
- 748 Zhong, D. L., 1998. , Paleotethysides in western Yunnan and Sichuan, China. Science Press, Beijing, pp.
749 9-215.
- 750 Zhou, J.C., Wang, X.L., Qiu, J.S., 2009. Geochronology of Neoproterozoic mafic rocks and sandstones
751 from northeastern Guizhou, South China: coeval arc magmatism and sedimentation. Precambrian

- 752 Research 170, 27-42.
- 753 Zhou, M.F., Kennedy, A.K., Sun, M., Malpas, J., Lesher, C.M., 2002a. Neoproterozoic arc-related mafic
754 intrusions along the northern margin of South China: implications for the accretion of Rodinia.
755 Journal of Geology 110, 611-618.
- 756 Zhou, M.F., Ma, Y.X., Yan, D.P., Xia, X.P., Zhao, J.H., Sun, M., 2006b. The Yanbian terrane (Southern
757 Sichuan Province, SW China): a Neoproterozoic arc assemblage in the western margin of the Yangtze
758 block. Precambrian Research 144, 19-38.
- 759 Zhou, M.F., Yan, D.P., Kennedy, A.K., Li, Y.Q., Ding, J., 2002b. SHRIMP U-Pb zircon
760 geochronological and geochemical evidence for Neoproterozoic arc-magmaism along the western
761 margin of the Yangtze Block, South China. Earth and Planetary Science Letters 196, 51-67.
- 762 Zhou, M.F., Yan, D.P., Wang, C.L., Qi, L., Kennedy, A., 2006a. Subduction-related origin of the 750 Ma
763 Xuelongbao adakitic complex (Sichuan Province, China): implications for the tectonic setting of the
764 giant Neoproterozoic magmatic event in South China. Earth and Planetary Science Letters 248,
765 286-300.
- 766 Zhu, W.G., Zhong, H., Deng, H.L., Wilson, A.H., Liu, B.G., Li, C.Y., Qin, Y., 2006. SHRIMP zircon
767 U-Pb age, geochemistry, and Nd-Sr isotopes of the Gaojiacun mafic-ultramafic intrusive complex,
768 Southwest China. International Geology Review 48, 650-668.
- 769 Zhu, W.G., Zhong, H., Li, X.H., Deng, H.L., He, D.F., Wu, K.W., Bai, Z.J., 2008. SHRIMP zircon U-Pb
770 geochronology, elemental, and Nd isotopic geochemistry of the Neoproterozoic mafic dykes in the
771 Yanbian area, SW China. Precambrian Research 164, 66-85.
- 772

772 **Figure Caption**

- 773 Fig.1. Simplified geotectonic map showing the Ailaoshan zone (modified after Leloup et al.,
 774 1995; Lin et al., 2012; Zhao and Cawood, 2012). (G) and (B) refer to the ages for
 775 granite and basalt and others from the volcanics from the sedimentary-volcanic
 776 sequence. The cited geochronological data are from Supplementary table 1.
- 777 Fig.2. (a) Schematic geological map of the Ailaoshan suture zone showing (b) the
 778 distribution of amphibolites at Jinping and (c) at Yuanyang.
- 779 Fig.3. Microscope photographs for the representative amphibolites along the Ailaoshan zone.
 780 (a) amphibolite 10HH-31A, (b) amphibolite 10HH-67A. Amp: amphibole, Pl:
 781 plagioclase, Cpx: clinopyroxene.
- 782 Fig.4. Zircon U-Pb concordia diagram for amphibolites along the Ailaoshan suture zone. (a)
 783 10HH-31A amphibolite at Qingjiao (Jinping), (b) 10HH-67A amphibolite at
 784 Yiwanshui (Yuanyang), and (c) 10HH-67B amphibolite at Yiwanshui (Yuanyang).
- 785 Fig.5. Plots of SiO₂ versus (a) MgO, (b) FeOt, (c) CaO, (d) Al₂O₃, (e) TiO₂, (f) P₂O₅, and MgO
 786 versus (g) Cr and (h) Ni for amphibolites from the Ailaoshan suture zone.
- 787 Fig.6. Classification plots of (a) Zr/TiO₂ versus Nb/Y (Winchester and Floyd, 1977); (b) La/Yb
 788 versus mg-number and, (c) Nb/U versus Nb (Kepezhinskas et al., 1996) for the amphibolites
 789 along the Ailaoshan zone. The fields of the island arc basalts and Nb-enrich basalt are from
 790 (Kepezhinskas et al., 1996). The data for ~1.0 Ga metabasite with the affinity to
 791 back-arc-basin basalt and Nb-enriched arc basalt from the Cathaysia Block are from Wang et
 792 al.(2013b). Symbols in (b-c) are the same as those in (a).
- 793 Fig.7. Chondrite-normalized REE patterns and primitive mantle-normalized incompatible element
 794 spidergrams for the amphibolites along the Ailaoshan suture zone. Abbreviations:
 795 SYB-Southern Yangtze Block; WYB-Western Yangtze Block; NYB-Northern Yangtze Block;
 796 EYB-Eastern Yangtze Block; CB-Cathaysia Block. The normalized values for the chondrite
 797 and primitive mantle are from Sun and McDonough (1989). Data for the Barren arc-volcanic
 798 rocks and East Scotia back-arc-basin are from Luhr and Haldar (2006) and Leat et al. (2000),
 799 respectively. OIB, N-MORB and E-MORB are after Sun and McDonough (1989).
 800 Nb-enriched basaltic andesite from Hispaniola and Yunkai are from Viruete et al. (2007) and

801 Zhang et al. (2012a), respectively. Panzhihua mafic rocks are from Zhao and Zhou (2007) and
 802 Li et al. (2006) and references therein. Hannan mafic rocks are from Zhao and Zhou (2009),
 803 Dong et al. (2011), Ling et al. (2003). Xiang-Gan mafic rocks are from Wang et al. (2008b), Li
 804 et al. (2008b) and references therein.

805 Fig.8. Plots of (a) Nb/La versus SiO₂, (b) ε_{Nd}(t) versus (⁸⁷Sr/⁸⁶Sr)_i (c) SiO₂ versus ε_{Nd}(t) (Wang et al.,
 806 2013a) and (d) 1000/Nd versus ε_{Nd}(t) (Zhang et al., 2012a). Data for the Neoproterozoic (~810
 807 Ma) mafic intrusions in Yanbian Terrane and Neoproterozoic gabbros in Panzhihua of the
 808 western Yangtze Block are from Zhou et al. (2006b) and Zhao and Zhou (2007). SC lines 1
 809 and 2 (red solid line) note source contamination of the depleted mantle and wedge with SCC
 810 crustal sediment, respectively. SC line 2 denotes the delamination of the SCB basement into
 811 the lithospheric mantle. CA lines 1 and 2 (pale blue dashed line) mean crustal assimilation en
 812 route for the depleted mantle- and wedge-derived magma with SCB crust, respectively. The
 813 modeling results show that the ~10-30 % average crustal materials are required to be involved
 814 in the MORB-derived magma by crustal contamination en route for matching the observed Nd
 815 isotopic compositions but failing to interpret the variation of Nb/La ratios for groups 1 and 2.

816 Fig.9. Discrimination diagrams of (a) Gd/Yb versus Nb/La (Zhang et al., 2012a), (b) Ba/Yb versus
 817 Nb/Yb (Pearce and Stern, 2006), and (c) Th/Yb versus Nb/Yb (Pearce, 2008) for the
 818 amphibolites along the Ailaoshan suture zone. Back-arc basalts modified by subduction
 819 components always plot between the MORB array and arc field and those of unaffected by
 820 subduction components mostly within the MORB array. Data for the arc rocks in the west
 821 Yangtze Block (~810 Ma), South Sandwich arc-Scotia BABB and Mariana arc and BAB are
 822 from Zhou et al. (2006b), Pearce and Stern (2006) and Pearce (2008), respectively.

823 Fig.10. (a) Nb/Th versus La/Nb. (b) Ce versus Yb (Hollings and Kerrich, 2004), (c) Ta/Yb versus
 824 Th/Yb (Pearce and Peate, 1995), and (d) Th/Nb versus Ce/Nb (Zhang et al., 2012a) for the
 825 amphibolites along the Ailaoshan zone.

826 Fig.11. Discrimination diagrams of (a) Nb/Zr versus Th/Zr (Zhao and Zhou, 2007), (b) Nb/Y versus
 827 Rb/Y (Kepezhinskaya et al., 1997), (c) Nb/U versus εNd (t) (Fan et al., 2010), and (d) Th/Nb
 828 versus Ba/Nb (Pearce and Stern, 2006) for the amphibolites along the Ailaoshan zone.

829 Fig.12. Age range of principal Neoproterozoic rocks around the Yangtze Block. Abbreviations:

830 SYB-Southern Yangtze Block; WYB-Western Yangtze Block; NYB-Northern Yangtze Block;
831 EYB-Eastern Yangtze Block; CB-Cathaysia Block; PS-PoSen; ALS-Ailaoshan;
832 DCS-Diancangshan; PZH-Panzhihua; KD-Kangding; BK-Bikou; HN-Hannan; DH-Donghai;
833 SX-Shangxi; SXW-Shuangxiwu; SQS-Shuangqiaoshan; BX-Banxi; CSP-Cangshuiyu;
834 LJX-Lengjiaxi; FJS-Fangjingshan; DZ-Danzhou; WY-Wuyi; YK-Yunkai. Numbers on data
835 points refer to the following sources: 1 Lin et al. (2012), 2 Liu et al. (2008a), 3 Qi et al. (2012),
836 4 Wang et al. (2011a), 5 Li et al. (2003b), 6 Zhou et al. (2002b), 7 Li et al. (2003a), 8 Sinclair
837 (2001), 9 Zhou et al. (2006b), 10 Zhao and Zhou (2007), 11 Zhu et al. (2006), 12 Zhu et al.
838 (2008), 13 Li et al. (2003c), 14 Du et al. (2007), 15 Li et al. (2002), 16 Ma et al. (1989), 17
839 Zhao et al. (2008), 18 Huang et al. (2008), 19 Roger and Calassou (1997), 20 Ling et al.
840 (2001), 21 Pei et al. (2009), 22 Zhao and Zhou (2008), 23 Xia et al. (2009), 24 Dong et al.
841 (2011), 25 Zhou et al. (2002a), 26 Zhao and Zhou (2009), 27 Dong et al. (2012), 28 Zhao et al.
842 (2010), 29 Zhang et al. (2000), 30 Zhao et al. (2006), 31 Zhang et al. (2004), 32 Yan et al.
843 (2004), 33 Wang et al. (2008c), 34 Ling et al. (2003), 35 Liu and Zhang. (2013), 36 Ma et al.
844 (1984), 37 Zhao et al. (2013), 38 Bao et al. (2008), 39 Zhang et al. (2006), 40 Chen et al.
845 (2013), 41 Xu et al. (2001), 42 Xu et al. (2006), 43 Liu et al. (2008b), 44 Chen et al. (2010),
846 45 Liu et al. (2004), 46 Chen et al. (2007), 47 Chen et al. (2003), 48 Hacker et al. (2006), 49
847 Hu et al. (2007), 50 Zheng et al. (2008), 51 Xue et al. (2010), 52 Li et al. (2010), 53 Wang et
848 al. (2012a), 54 Zhang et al. (2012c), 55 Li et al. (2008a), 56 Wang et al. (2008a), 57 Li et al.
849 (2008b), 58 Wu et al. (2010), 59 Wang et al. (2007b), 60 Zhang et al. (2012b), 61 Zhang et al.
850 (2013a), 62 Wang et al. (2008b), 63 Zhou et al. (2009), 64 Ge et al. (2001), 65 Yin et al.
851 (2013), 66 Wang et al. (2006), 67 Zeng et al. (2005), 68 Li (1999), 69 Wang et al. (2010), 70
852 Wang et al. (2013b), 71 Zhang et al. (2012a), 72 Ye et al. (2007), 73 Li et al. (2009b), 74 Shu
853 et al. (2011), 75 Qin et al. (2006), 76 Zhang et al. (1998).
854
855

Table 1 SIMS and LA-ICP-MS zircon U-Pb isotopic analyses of the representative amphibolites along the Ailaoshan zone

Spot	Element(ppm)		Th/U	Isotope ratio						Age (Ma)			
	^{232}Th	^{238}U		$^{207}\text{Pb}/^{206}\text{Pb}$	$\pm 1\sigma$	$^{207}\text{Pb}/^{235}\text{U}$	$\pm 1\sigma$	$^{206}\text{Pb}/^{238}\text{U}$	$\pm 1\sigma$	$^{207}\text{Pb}/^{206}\text{Pb}$	$\pm 1\sigma$	$^{206}\text{Pb}/^{238}\text{U}$	$\pm 1\sigma$
10HH-31A	amphibolite, Qingjiao, Jinping in western Yunnan (LA-ICPMS dating method)												
10HH-31A-01	244	322	0.76	0.0655	0.002	1.1839	0.03	0.1311	0.003	790	48	794	15
10HH-31A-02	277	560	0.49	0.0647	0.002	0.9885	0.02	0.1108	0.002	765	57	677	14
10HH-31A-03	136	154	0.88	0.0759	0.004	1.3726	0.07	0.1311	0.005	1093	112	794	26
10HH-31A-04	252	369	0.68	0.0703	0.003	1.2151	0.04	0.1253	0.003	937	73	761	17
10HH-31A-05	238	326	0.73	0.0658	0.002	1.2238	0.03	0.1349	0.003	799	62	816	17
10HH-31A-06	536	504	1.07	0.0671	0.002	1.2264	0.03	0.1325	0.003	841	52	802	15
10HH-31A-07	268	332	0.81	0.0671	0.002	1.2660	0.04	0.1368	0.003	841	68	827	18
10HH-31A-08	558	1138	0.49	0.0660	0.001	1.2007	0.02	0.1320	0.002	805	39	799	14
10HH-31A-09	269	305	0.88	0.0668	0.002	1.2685	0.04	0.1377	0.003	832	68	832	18
10HH-31A-10	345	386	0.89	0.0649	0.002	1.1933	0.03	0.1334	0.003	770	52	807	15
10HH-31A-11	413	480	0.86	0.0644	0.002	1.1721	0.03	0.1321	0.003	753	56	800	16
10HH-31A-12	245	401	0.61	0.0686	0.002	1.2742	0.03	0.1348	0.003	885	51	815	15
10HH-31A-13	244	313	0.78	0.0686	0.003	1.2478	0.06	0.1320	0.004	885	101	800	22
10HH-31A-14	221	265	0.83	0.0683	0.003	1.2078	0.04	0.1282	0.003	879	75	778	17
10HH-31A-15	254	323	0.79	0.0710	0.003	1.2629	0.04	0.1291	0.003	957	74	783	18
10HH-31A-16	208	117	1.78	0.0706	0.004	1.2572	0.07	0.1293	0.004	944	121	784	25
10HH-31A-17	299	336	0.89	0.0630	0.003	1.2042	0.05	0.1388	0.004	708	89	838	20
10HH-31A-18	274	333	0.82	0.0679	0.002	1.2624	0.04	0.1350	0.003	865	65	816	17
10HH-31A-19	311	425	0.73	0.0655	0.002	1.1984	0.03	0.1328	0.003	791	54	804	15
10HH-31A-20	397	419	0.95	0.0700	0.002	1.2746	0.04	0.1321	0.003	929	61	800	16
10HH-31A-21	278	442	0.63	0.0667	0.002	1.2341	0.03	0.1343	0.003	829	56	812	16
10HH-31A-22	313	381	0.82	0.0665	0.002	1.2368	0.04	0.1351	0.003	821	66	817	17
10HH-31A-23	174	355	0.49	0.0689	0.002	1.2384	0.04	0.1304	0.003	897	66	790	17
10HH-31A-24	571	591	0.97	0.0661	0.001	1.1964	0.02	0.1314	0.002	810	46	796	14
10HH-67A	amphibolite, Yiwanshui, Yuanyang in western Yunnan (SIMS dating method)												
10HH-67A-01	516	662	0.78	0.0633	1.02	0.9332	1.83	0.1069	1.52	719	22	655	9
10HH-67A-02	1332	1992	0.67	0.0471	2.98	0.1270	3.33	0.0196	1.50	54	69	125	2
10HH-67A-03	120	224	0.54	0.0668	1.41	1.0776	2.06	0.1170	1.50	832	29	713	10
10HH-67A-04	48	520	0.09	0.0691	1.81	1.2949	2.36	0.1359	1.50	902	37	821	12
10HH-67A-05	87	139	0.62	0.0519	2.29	0.3314	2.76	0.0463	1.53	281	52	292	4
10HH-67A-06	225	302	0.75	0.0493	5.39	0.0353	5.66	0.0052	1.75	162	121	33	1
10HH-67A-07	299	486	0.62	0.0566	2.48	0.6198	2.90	0.0794	1.50	476	54	493	7
10HH-67A-08	108	284	0.38	0.0649	0.87	1.2175	1.75	0.1360	1.52	772	18	822	12
10HH-67A-09	264	501	0.53	0.0666	0.74	1.2082	1.67	0.1316	1.50	825	15	797	11
10HH-67A-10	527	561	0.94	0.1273	0.42	5.7767	1.56	0.3292	1.51	2061	7	1834	24
10HH-67A-11	145	390	0.37	0.0658	0.74	1.2221	1.67	0.1347	1.50	800	15	815	11
10HH-67A-12	312	302	1.03	0.0637	0.97	1.0159	1.79	0.1157	1.50	732	20	706	10

10HH-67A-13	173	196	0.88	0.0647	1.13	1.0889	1.88	0.1220	1.50	766	24	742	11
10HH-67A-14	325	835	0.39	0.0723	0.51	1.2108	1.59	0.1215	1.50	994	10	739	10
10HH-67A-15	469	1238	0.38	0.0676	0.53	1.1006	1.60	0.1180	1.50	857	11	719	10
10HH-67A-16	3400	12288	0.28	0.0466	0.82	0.0317	1.71	0.0049	1.50	31	20	32	0
10HH-67B amphibolite, Yiwanshui, Yuanyang in western Yunnan (LA-ICPMS dating method)													
10HH-67B-01	105	112	0.94	0.0672	0.002	1.1298	0.03	0.1219	0.003	856	58	741	18
10HH-67B-02	206	355	0.58	0.0781	0.002	1.7348	0.04	0.1610	0.004	1150	50	962	23
10HH-67B-03	71	156	0.45	0.0662	0.002	1.2276	0.03	0.1346	0.003	813	49	814	20
10HH-67B-04	542	901	0.60	0.0659	0.002	1.0001	0.03	0.1099	0.003	806	54	672	18
10HH-67B-05	229	191	1.20	0.0678	0.002	1.2577	0.03	0.1346	0.003	861	56	814	20
10HH-67B-06	88	293	0.30	0.0541	0.001	0.2888	0.01	0.0388	0.001	372	57	245	6
10HH-67B-07	55	566	0.10	0.0679	0.002	1.2599	0.03	0.1345	0.003	865	52	814	20
10HH-67B-08	144	178	0.81	0.0656	0.002	1.2153	0.03	0.1343	0.003	794	58	812	19
10HH-67B-09	149	485	0.31	0.0672	0.002	1.2513	0.03	0.1351	0.003	843	52	817	20
10HH-67B-10	380	416	0.91	0.1291	0.003	6.6491	0.17	0.3738	0.010	2087	44	2047	46
10HH-67B-11	211	891	0.24	0.0662	0.002	1.0456	0.03	0.1145	0.003	813	52	699	18
10HH-67B-12	108	323	0.33	0.0666	0.002	1.2377	0.03	0.1348	0.003	833	52	815	20
10HH-67B-13	426	634	0.67	0.0598	0.002	0.6995	0.03	0.0835	0.002	594	56	517	15
10HH-67B-14	79	117	0.67	0.0553	0.001	0.3733	0.01	0.0491	0.001	433	59	309	8
10HH-67B-15	72	152	0.47	0.0556	0.001	0.3795	0.01	0.0496	0.001	435	62	312	8
10HH-67B-16	323	393	0.82	0.0472	0.001	0.0354	0.00	0.0055	0.000	61	63	35	1
10HH-67B-17	57	155	0.36	0.0660	0.002	1.2220	0.03	0.1343	0.003	806	53	812	20
10HH-67B-18	294	1155	0.25	0.0734	0.002	1.3669	0.03	0.1351	0.003	1033	52	817	19
10HH-67B-19	332	539	0.62	0.1897	0.005	11.9528	0.30	0.4568	0.012	2740	41	2425	51
10HH-67B-20	416	593	0.70	0.0596	0.002	0.6629	0.02	0.0806	0.002	591	28	500	12
10HH-67B-21	84	182	0.46	0.0689	0.002	1.2766	0.03	0.1342	0.003	896	54	812	19
10HH-67B-22	199	708	0.28	0.0600	0.002	0.6005	0.02	0.0725	0.002	606	54	451	11
10HH-67B-23	83	179	0.46	0.0652	0.002	1.2045	0.03	0.1340	0.003	789	52	811	19
10HH-67B-24	108	372	0.29	0.0779	0.002	1.7808	0.05	0.1656	0.004	1146	50	988	23
10HH-67B-25	108	1013	0.11	0.0603	0.002	0.6357	0.02	0.0764	0.002	617	86	474	12
10HH-67B-26	230	1608	0.14	0.0640	0.002	0.8241	0.02	0.0933	0.002	743	54	575	14

Table 2 Major element (in wt %) and trace element (in ppm) compositions of the Neoproterozoic amphibolites along the Ailaoshan suture zone

Sample	Group 1					Group 2						
	10HH-31A	10HH-31C	10HH-31D	10HH-31E	10HH-31F	10HH-67A	10HH-67B	10HH-67D	10HH-67F	10HH-69A	10HH-69C	10HH-69E
SiO ₂	51.45	49.34	47.61	47.08	50.92	48.55	48.63	49.03	48.87	47.29	46.81	46.85
TiO ₂	0.37	0.46	0.71	0.76	0.56	1.84	1.67	1.71	1.84	2.22	2.21	2.20
Al ₂ O ₃	15.15	14.56	14.43	13.16	14.81	11.89	10.77	10.84	11.97	14.38	14.40	14.47
Fe ₂ O ₃ ^T	7.88	8.01	8.95	9.94	8.81	12.90	12.58	12.85	13.13	14.54	14.57	14.48
MgO	8.82	11.02	11.45	12.07	9.21	10.09	11.30	11.57	9.97	6.83	7.03	6.98
CaO	12.47	12.57	12.94	13.59	11.07	10.70	10.68	9.99	10.33	11.61	12.00	11.88
K ₂ O	0.75	0.83	0.81	0.59	0.81	0.23	0.16	0.16	0.25	0.62	0.53	0.46
Na ₂ O	2.42	2.37	2.21	2.18	2.88	2.03	1.51	1.46	2.01	1.17	1.15	1.20
MnO	0.14	0.14	0.13	0.14	0.13	0.17	0.15	0.16	0.16	0.19	0.20	0.20
P ₂ O ₅	0.04	0.03	0.06	0.02	0.04	0.24	0.21	0.21	0.24	0.29	0.28	0.29
L.O.I	0.43	0.61	0.58	0.41	0.58	1.21	2.16	1.87	1.11	0.70	0.66	0.85
Total	99.93	99.94	99.88	99.94	99.82	99.86	99.83	99.85	99.89	99.85	99.85	99.85
mg-number	72	76	75	74	71	65	68	68	64	52	53	53
Sc	36.9	35.2	37.9	39.5	363.4	41.2	43.9	43.2	40.5	35.2	37.9	36.6
V	147	160	136	173	141	311	301	300	304	326	354	337
Cr	220	220	501	649	301	438	561	556	417	103	108	104
Co	32.7	35.1	31.1	38.6	30.8	56.4	57.4	57.3	53.2	50.2	52.5	48.5
Ni	9.7	15.4	18.7	21.5	11.9	119.3	127.0	130.4	116.7	100.3	105.3	99.9
Ga	14.2	14.9	15.2	15.9	13.5	16.3	14.9	14.9	16.2	17.7	18.2	18.4
Rb	10.6	12.6	15.9	21.1	8.5	5.1	2.0	2.1	6.0	11.8	19.7	12.7
Sr	432	399	373	308	406	458	303	298	487	238	278	242
Y	19.2	19.7	19.8	19.9	19.0	21.6	20.3	19.4	22.5	23.0	24.8	23.6
Zr	48.3	49.2	52.7	57.9	45.1	142.0	131.4	129.8	148.2	140.6	145.8	141.1
Nb	4.07	3.26	4.32	5.22	3.19	16.19	14.37	14.28	16.00	16.61	17.64	18.43
Cs	0.65	0.70	0.71	0.76	0.57	0.27	0.07	0.06	0.34	1.18	1.64	0.98

Ba	139.2	141.5	159.3	194.2	110.5	76.9	31.1	30.5	137.2	138.6	217.0	129.7
La	12.67	14.35	14.05	14.82	11.98	20.19	18.22	18.62	21.00	20.96	22.56	21.89
Ce	28.23	28.34	28.94	28.49	25.22	46.27	41.36	41.75	47.04	49.28	50.77	48.84
Pr	3.89	4.01	4.16	4.21	3.52	6.30	5.62	5.70	6.24	7.02	6.87	6.55
Nd	16.75	18.46	19.28	20.19	14.21	27.17	24.12	24.56	27.72	26.89	28.72	27.38
Sm	3.70	3.98	4.10	4.12	3.61	5.58	5.11	5.09	5.67	5.46	5.97	5.61
Eu	0.87	0.80	0.78	0.72	0.83	1.76	1.64	1.58	1.79	1.81	1.91	1.79
Gd	3.45	3.43	3.42	3.50	3.44	5.14	4.80	4.92	5.37	5.27	5.73	5.39
Tb	0.60	0.52	0.59	0.60	0.56	0.84	0.78	0.77	0.87	0.86	0.92	0.88
Dy	3.41	3.43	3.47	3.52	3.40	4.34	4.18	4.16	4.48	4.95	5.05	4.84
Ho	0.69	0.70	0.71	0.71	0.69	0.86	0.83	0.81	0.89	1.11	1.01	0.98
Er	1.80	1.79	1.80	1.82	1.78	2.15	2.06	2.04	2.18	2.57	2.55	2.48
Tm	0.26	0.26	0.27	0.28	0.23	0.30	0.30	0.28	0.31	0.38	0.37	0.37
Yb	1.76	1.76	1.77	1.80	1.73	1.94	1.81	1.82	2.00	2.30	2.32	2.29
Lu	0.28	0.28	0.26	0.28	0.27	0.29	0.27	0.27	0.30	0.33	0.36	0.34
Hf	1.27	1.51	1.70	1.80	1.39	3.88	3.57	3.50	3.95	3.87	3.91	3.65
Ta	0.31	0.32	0.34	0.39	0.29	1.11	1.01	1.00	1.16	1.20	1.27	1.21
Pb	9.83	9.93	11.00	11.59	8.45	5.15	3.71	4.37	5.16	13.37	13.46	13.23
Th	1.26	1.38	1.50	1.63	1.14	2.36	2.12	2.03	2.46	2.90	3.06	2.93
U	1.06	1.23	1.29	1.54	0.81	0.55	0.49	0.45	0.56	0.65	0.64	0.65
ΣREE	78.36	82.11	83.59	85.05	71.47	123.13	111.09	112.37	125.87	129.20	135.10	129.61

Table 3 Sr-Nd isotopic compositions of the amphibolites along the Ailaoshan suture zone

Sample	Sm	Nd	Rb	Sr	$^{147}\text{Sm}/^{144}\text{Nd}$	$^{143}\text{Nd}/^{144}\text{Nd}$	2σ	$(^{143}\text{Nd}/^{144}\text{Nd})_i$	$^{87}\text{Rb}/^{86}\text{Sr}$	$^{87}\text{Sr}/^{86}\text{Sr}$	2σ	$(^{87}\text{Sr}/^{86}\text{Sr})_i$	ϵ_{Nd}
Group 1													
10HH-31A	3.70	16.75	10.64	432.40	0.1334	0.512129	13	0.511429	0.0712	0.707009	11	0.706196	-3.45
10HH-31C	3.98	18.46	12.68	498.50	0.1304	0.512186	13	0.511502	0.0736	0.706758	13	0.705917	-2.04
10HH-31D	4.10	19.28	15.92	532.70	0.1284	0.512109	11	0.511435	0.0865	0.705917	13	0.704929	-3.34
10HH-31F	3.61	14.21	8.49	405.60	0.1537	0.512263	10	0.511457	0.0606	0.707319	12	0.706627	-2.91
Group 2													
10HH-67A	5.58	27.17	5.11	457.70	0.1242	0.512476	8	0.511814	0.0323	0.706913	13	0.706537	4.39
10HH-67D	5.09	24.56	2.12	297.50	0.1253	0.512476	6	0.511808	0.0206	0.707234	13	0.706995	4.28
10HH-69A	5.46	26.89	11.85	238.40	0.1228	0.512461	8	0.511806	0.1438	0.709238	12	0.707568	4.24
10HH-69E	5.61	27.38	12.73	242.40	0.1238	0.512457	8	0.511795	0.1520	0.712167	12	0.710398	4.08

Highlights

- Amphibolites in the Ailaoshan tectonic zone give U-Pb age of 815~800 Ma.
- They originated from a metasomatised source or slab-melt modified wedge.
- The formation is related with an arc-back-arc setting.
- The South China Craton located at the margin of Rodinia.

Accepted Manuscript

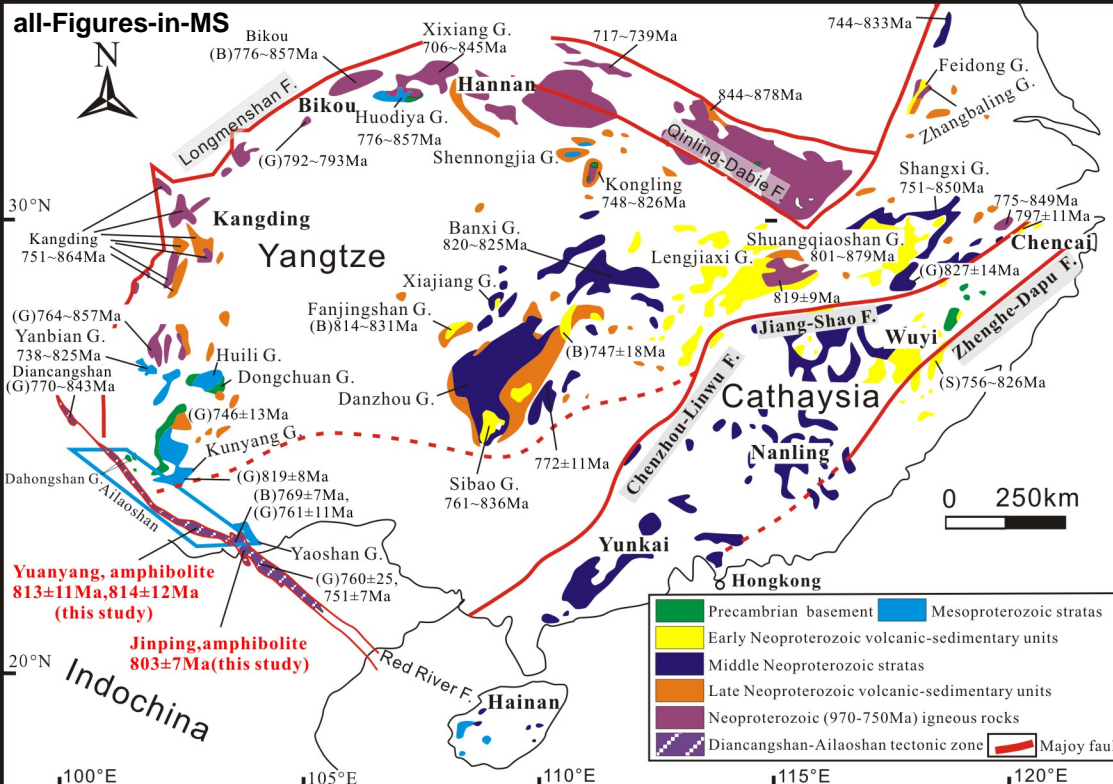


Fig.1 Y-F Cai and coauthors

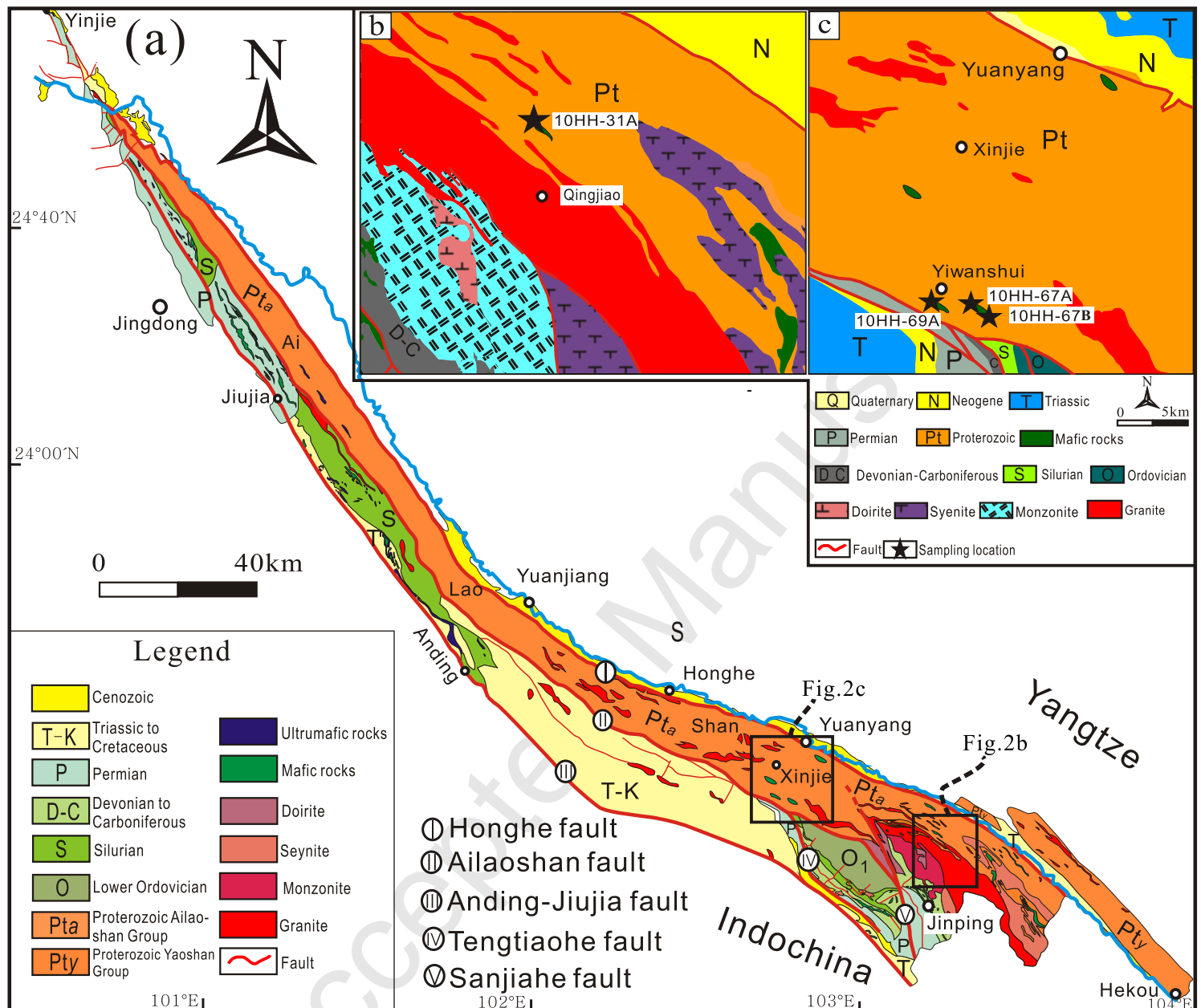


Fig.2 Y-F Cai and coauthors

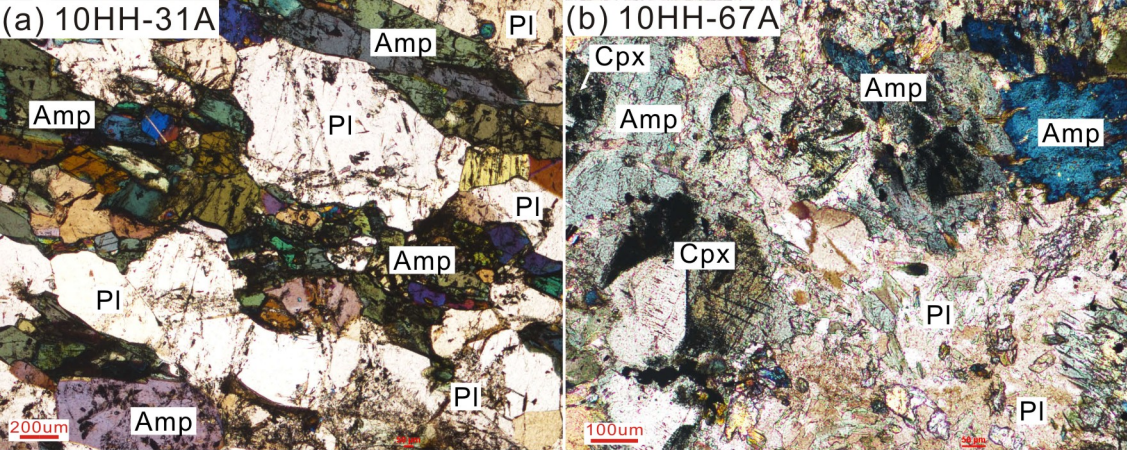


Fig.3 Y-F Cai and coauthors

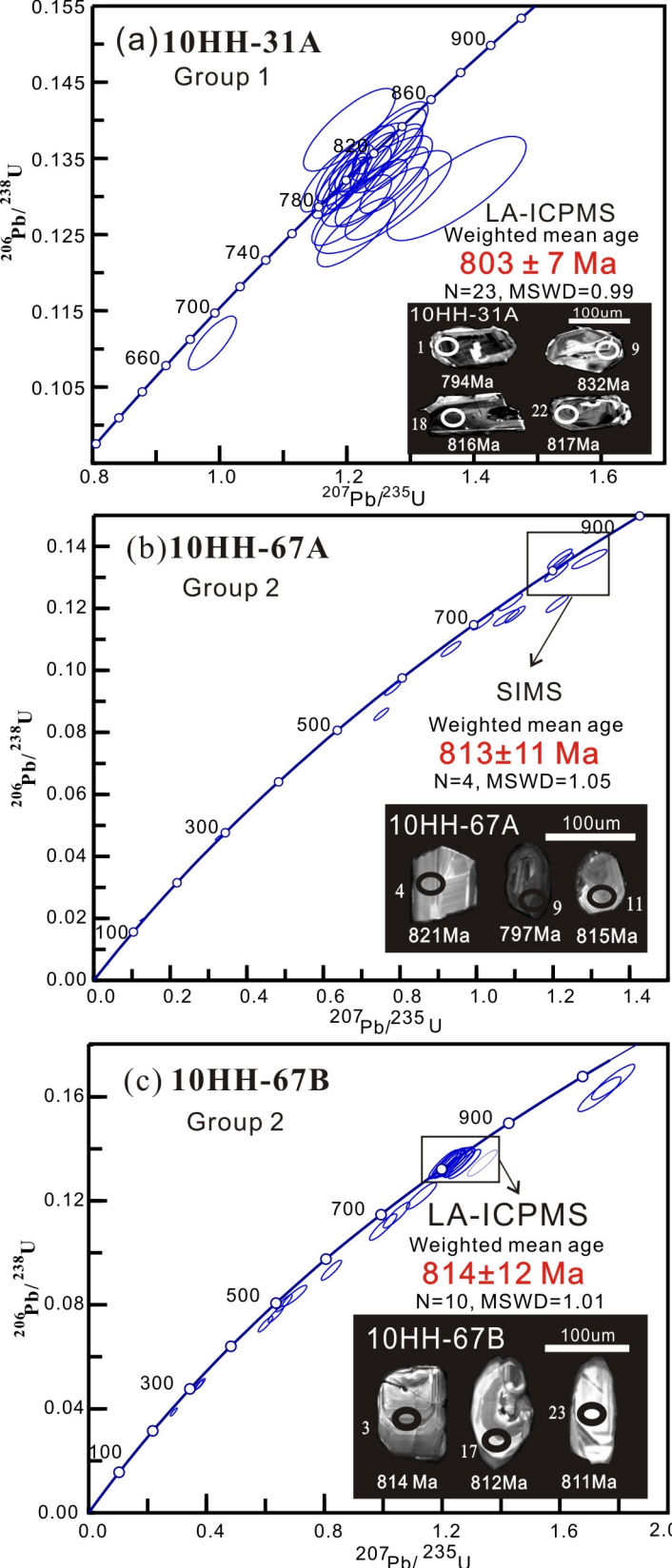


Fig.4 Y-F Cai and coauthors

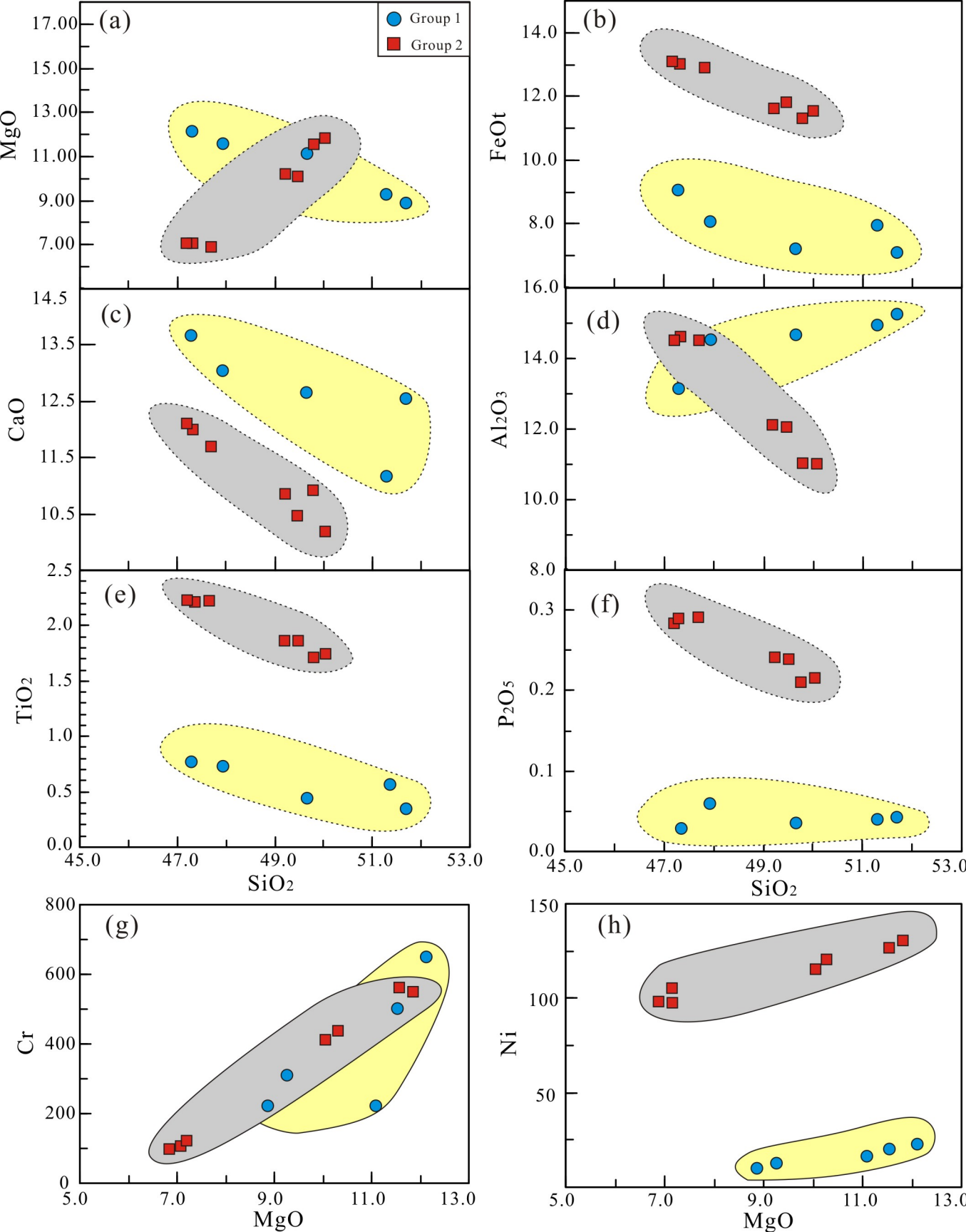


Fig.5 Y-F Cai and coauthors

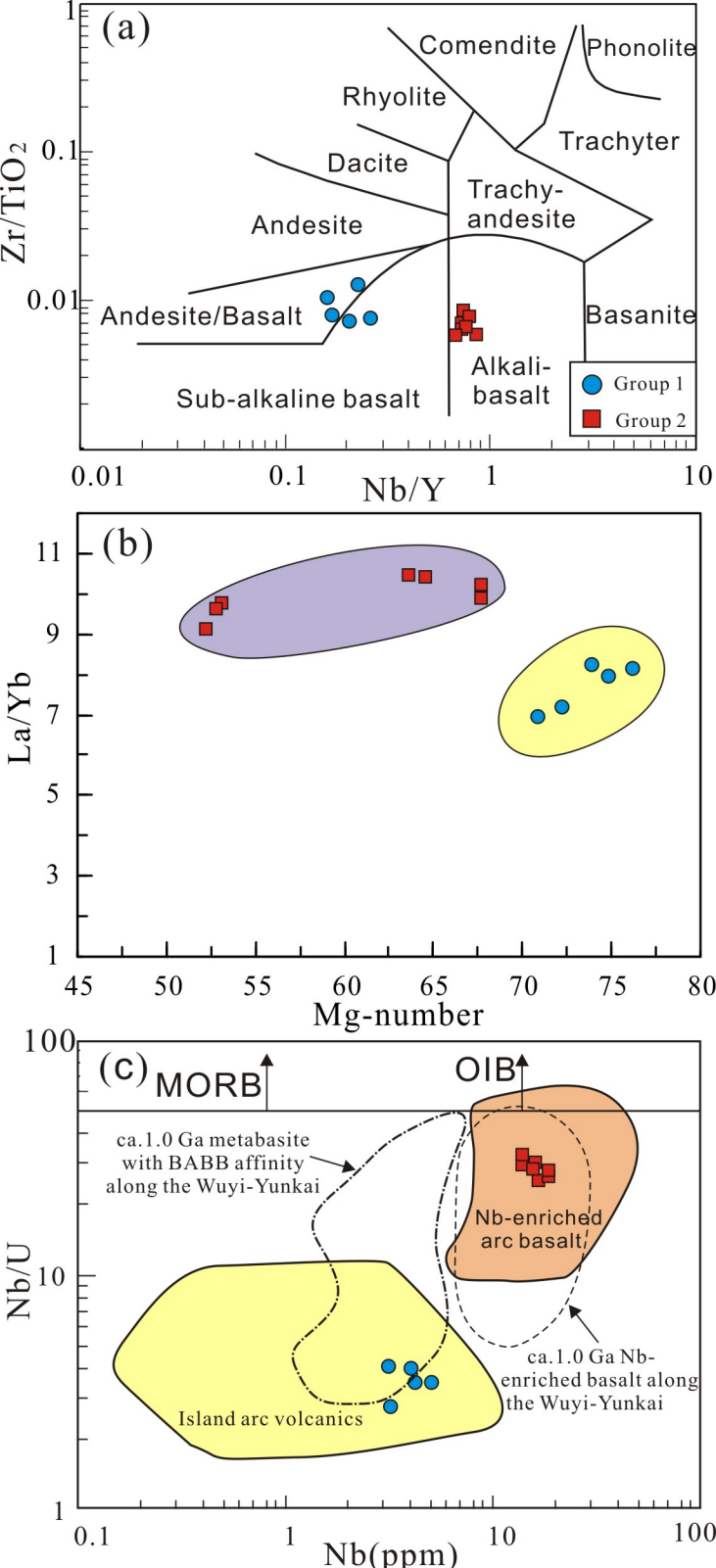


Fig.6 Y-F Cai and coauthors

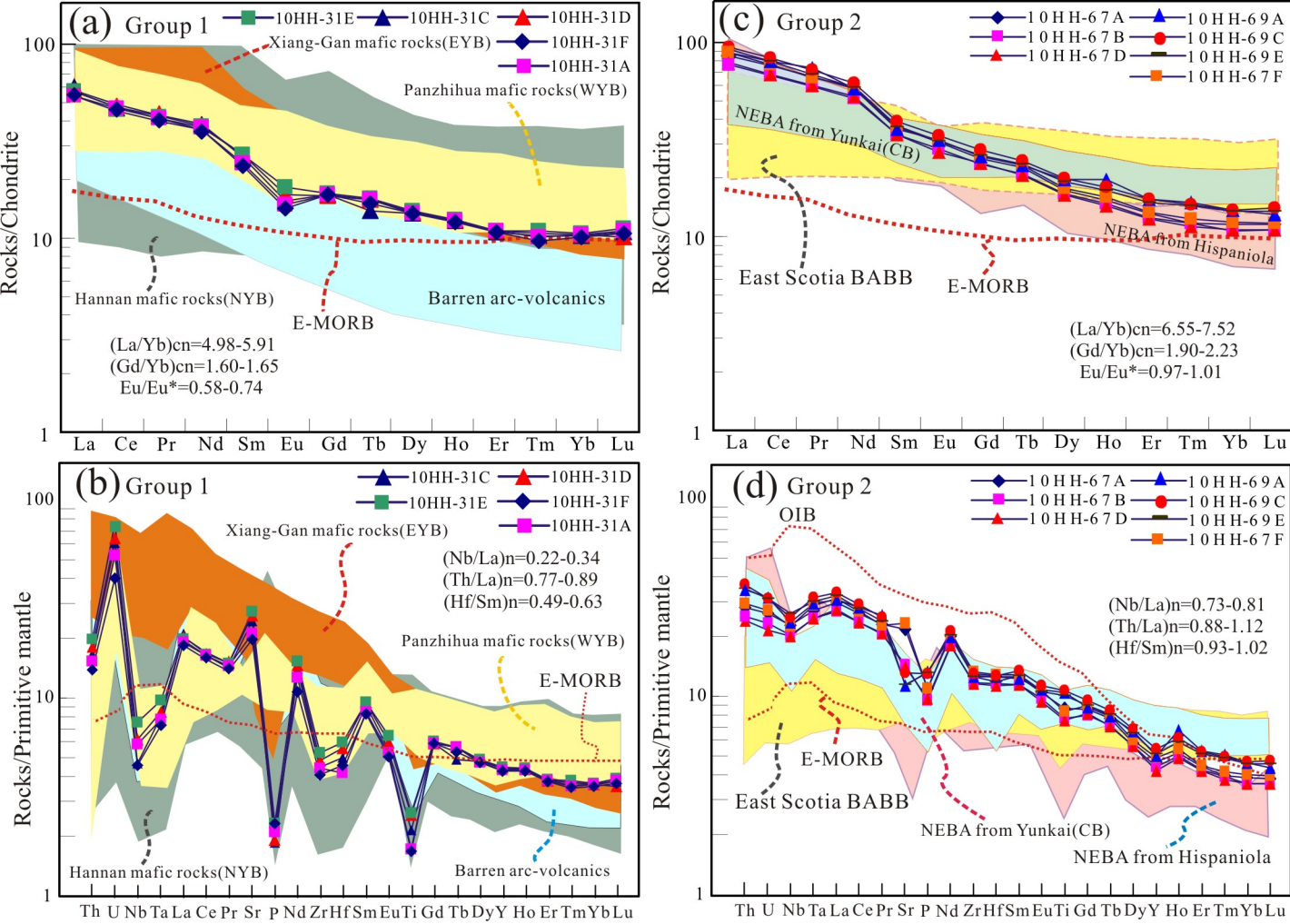


Fig.7 Y-F Cai and coauthors

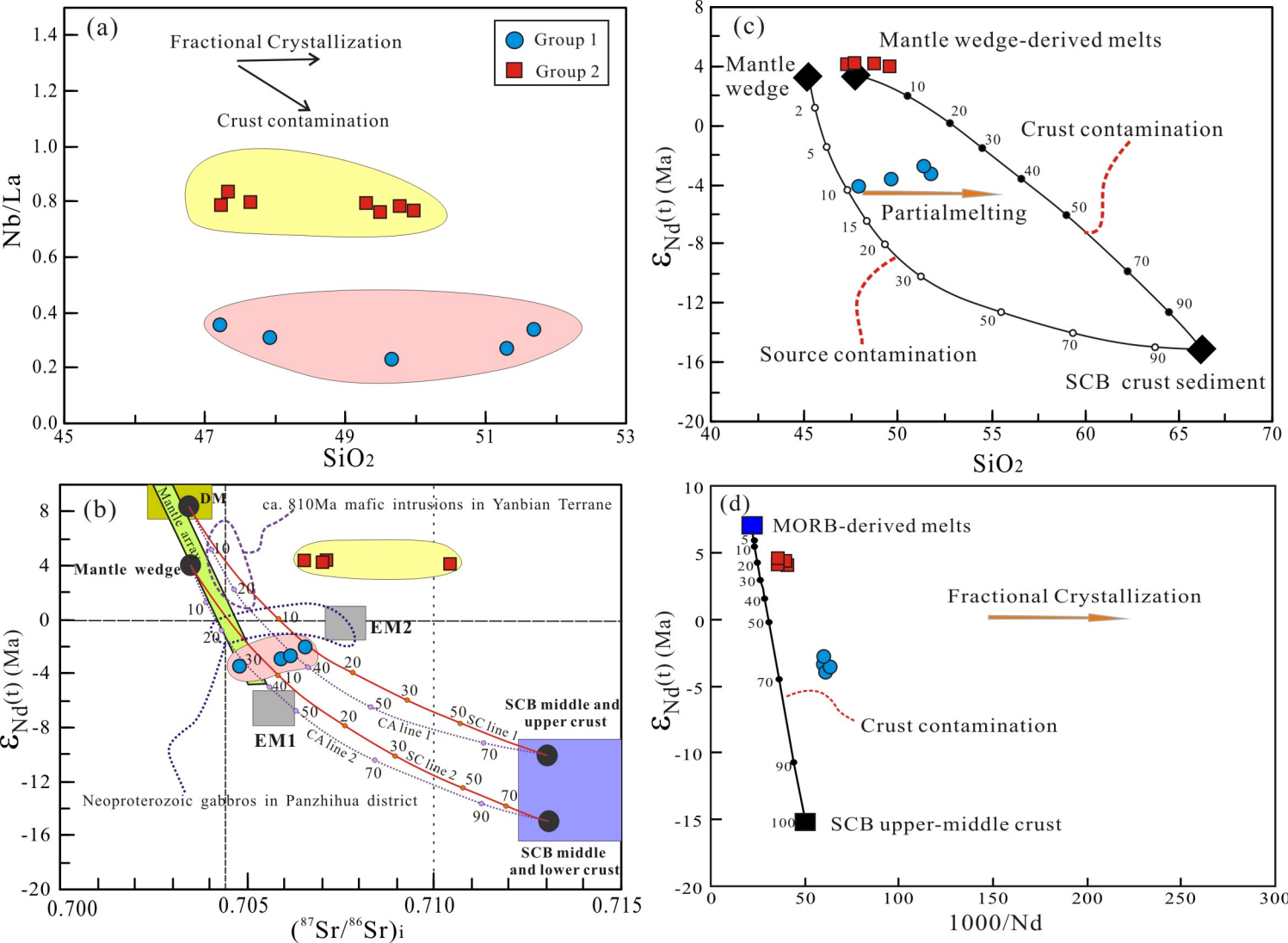


Fig.8 Y-F Cai and coauthors

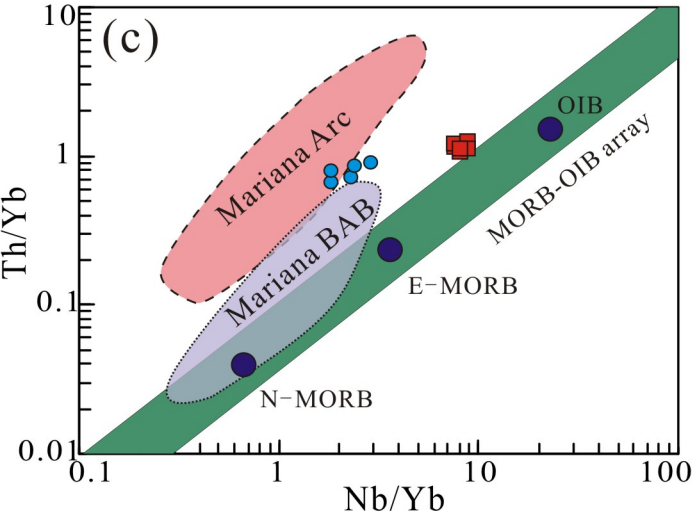
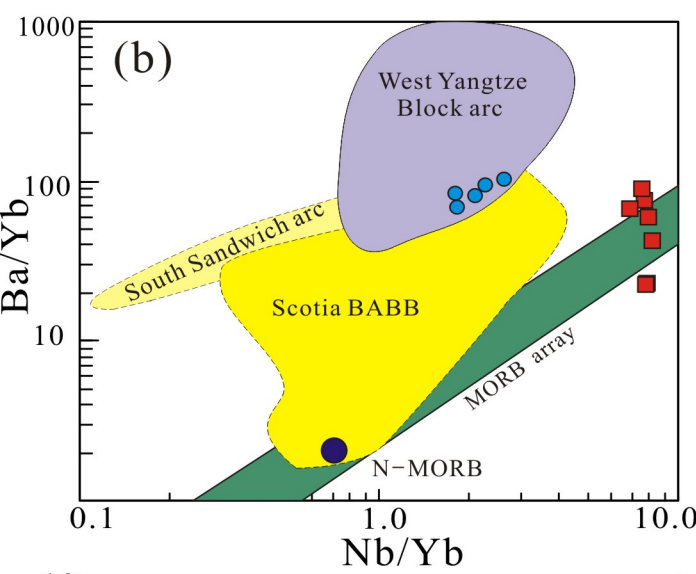
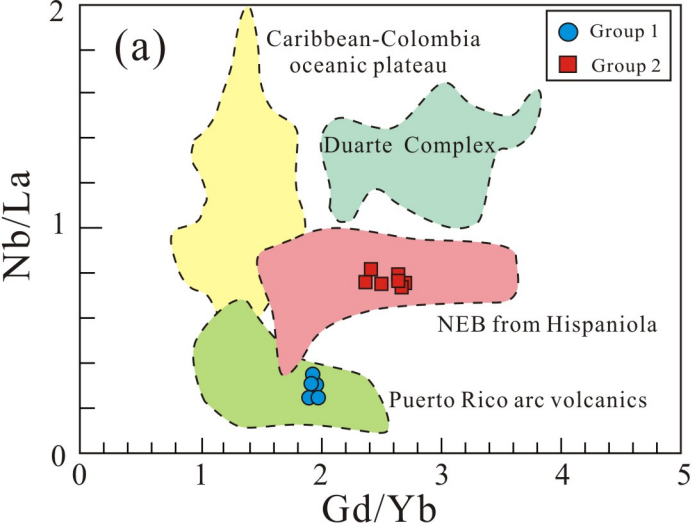


Fig.9 Y-F Cai and coauthors

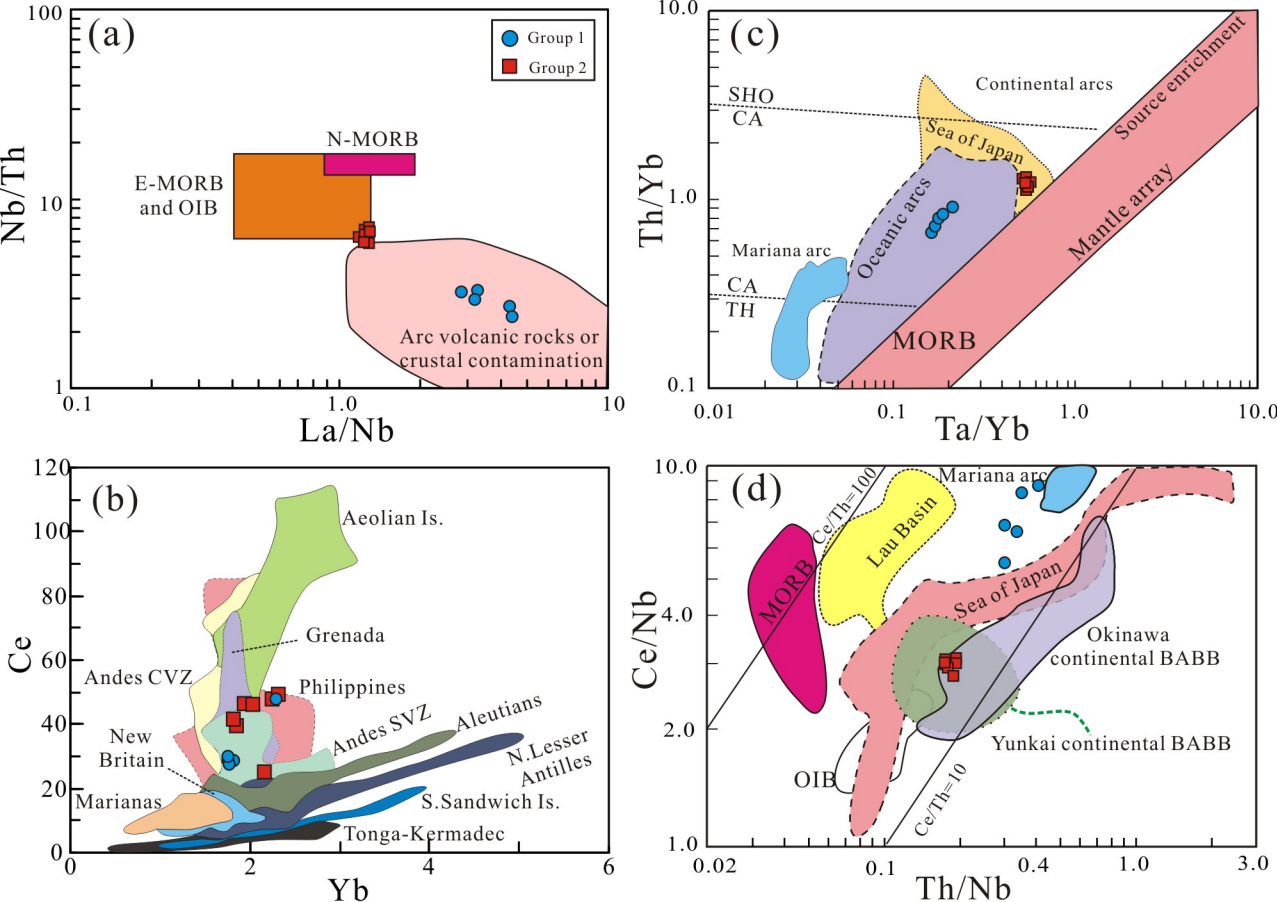


Fig.10 Y-F Cai and coauthors

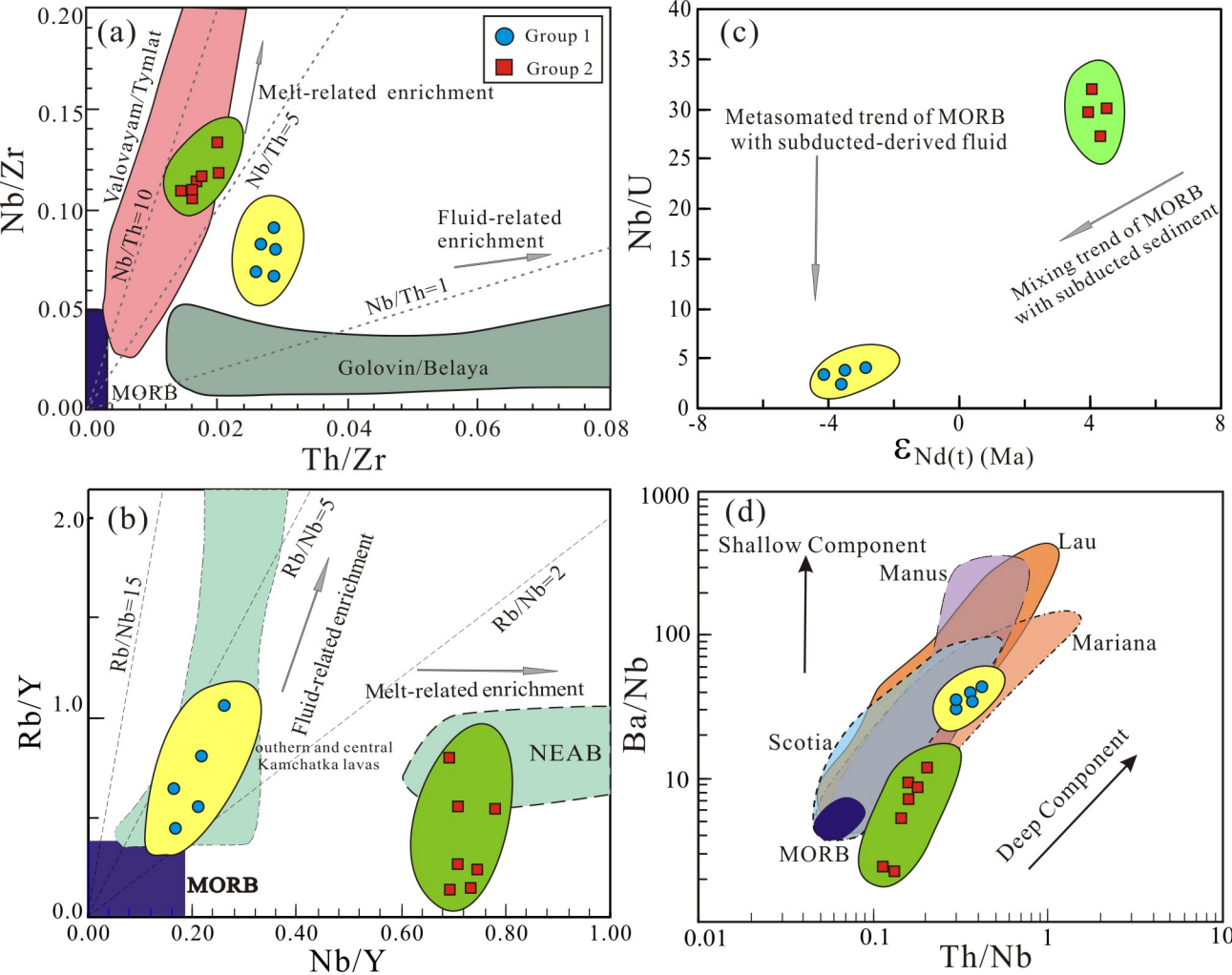


Fig.11 Y-F Cai and coauthors

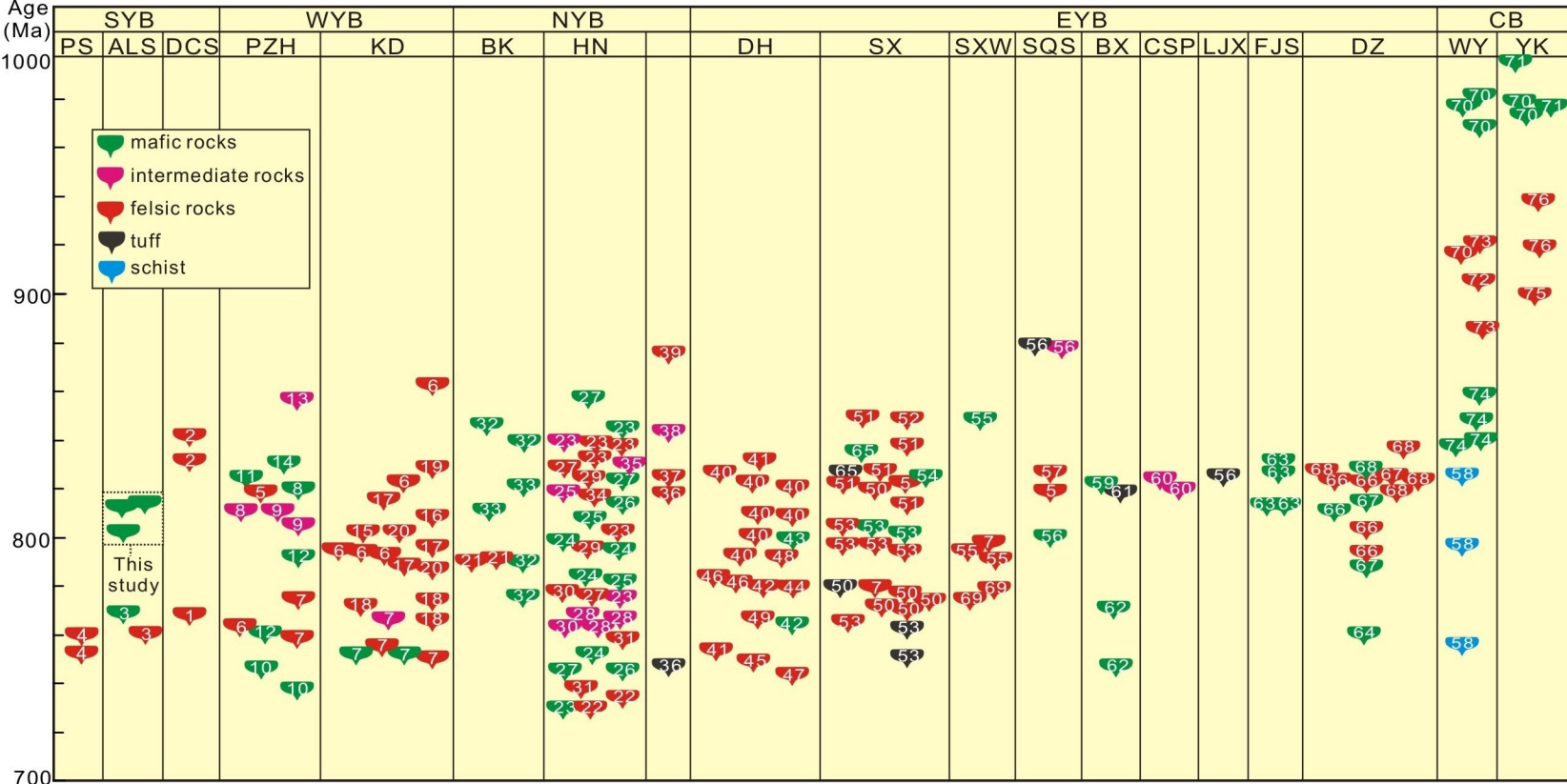


Fig.12 Y-F Cai and coauthors